LOCALIZATION OF SHORT CIRCUIT FAULTS

IN THE POWER DISTRIBUTION NETWORK

by

OMKAR DEEPAK LIMAYE

Presented to the Faculty of the Graduate School of

The University of Texas at Arlington in Partial Fulfillment

of the Requirements

for the Degree of

MASTER OF SCIENCE IN ELECTRICAL ENGINEERING

THE UNIVERSITY OF TEXAS AT ARLINGTON

December 2011

ACKNOWLEDGEMENTS

ABSTRACT

LOCALIZATION OF SHORT CIRCUIT FAULTS

IN THE POWER DISTRIBUTION NETWORK

Omkar Deepak Limaye, M.S.

The University of Texas at Arlington, 2011

Supervising Professor: Mingyu Lu

This thesis summarizes the research efforts on localizing short-circuit faults in power distribution networks. Specifically, an experimental testbed is constructed to emulate realistic power distribution networks; various short-circuit faults are artificially created in the testbed; voltages/currents are measured over the testbed; and finally, fault localization is achieved by analyzing the measurement data.

Two types of power distribution networks are analyzed: serial/radial and grid/mesh networks. In the serial network, a scheme based on terminal voltage and current measurements is developed. Two voltage profiles, namely "forward voltage profile" and "backward voltage profile," are plotted and their intersection is estimated as the fault location. This algorithm is found effective to provide accurate results for different fault impedances. In the case of grid/mesh network, two novel fault localization algorithms, "signature pattern recognition" and "sparse sensing," are implemented. They are both validated by extensive experimental data. The accuracy and robustness of the two algorithms are compared. It is observed that, standard voltage measurements at a small number of pre-selected nodes suffice to localize the faults

precisely; and hence, our fault localization scheme is of low cost. In addition, the algorithms are

found to be highly efficient: typically, fault localization is completed in less than 50 ms.

TABLE OF CONTENTS

LIST OF ILLUSTRATIONS

LIST OF TABLES

CHAPTER 1

INTRODUCTION

1.1 Motivation

Electric power is a critical resource in today's world. Compared to other natural or man-made disasters, electric power outage produces much more severe consequences (see Figure 1.1). Hence, it is extremely important to maintain the electric power service with a high level of reliability. If electric power outage occurs due to any abnormal conditions, its extent and duration must be controlled to be minimal. One of the principal missions of the utilities industry to build reliable power system protection and restoration schemes.
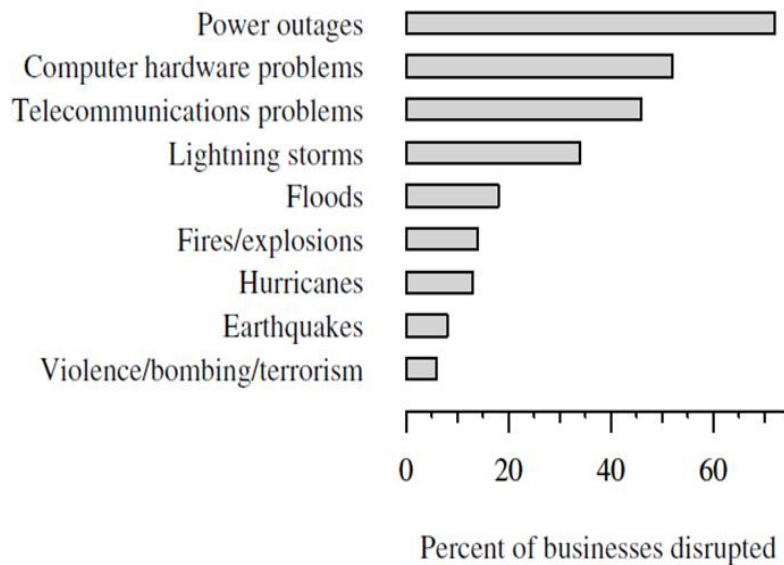
Figure 1.1 Percent of U.S. businesses disrupted by the given problem. (Data from [Rodentis, 1999].) [1]

Long-duration service interruptions constitute the primary part of "reliability statistics" of power systems, which are the foundations for the utilities and regulators to assess the quality of electric power service. Faults on the power distribution networks are found to be the reasons of most long-duration interruptions [1], and further, most of the severe power outages. A fault is defined as follows:

Fault : A physical condition that causes a device, a component, or an element to fail to perform in a required manner; for example, a short circuit or a broken wire [2].

Available statistical data indicate that, Consolidated Edison of New York (Con Edison) experiences more than 1600 failures on its distribution feeders and 1000 arcing faults on its secondary distribution system each year [3]. These faults led to cable burnouts, and in turn, resulted in costly repairs as well as hazard to the public safety.

Clearly, accurate and efficient fault localization techniques play an important role in the power systems [4]. Precise localization of temporary faults can prevent them from developing into permanent failures; and, localizing permanent faults can help resolving the problems and, reducing the interruption time [5]. Moreover, fault localization is always valuable to identifying potential faults/failures and improving the power system's reliability [6].

Three complications in power distribution networks make fault location a difficult task. First, the network is fed by power distribution circuits via multiple injection points. Hence it is virtually impossible to track the distribution circuits to pinpoint the faults. Second, although the faults do have tremendous impacts to their neighborhoods, typically they do not bring up drastic disturbances to the overall behavior of the network, especially at their initial stages. Third, the faults' signatures are usually attenuated by the large number of loads in the network.

A fault in power distribution networks almost always involves a short circuit between energized phase conductors or between a phase and ground. The term "fault" is often used synonymously with the term "short circuit" defined as:

Short circuit: An abnormal connection (including an arc) of relatively low impedance, whether made accidentally or intentionally, between two points of different potential [2][1].

This thesis aims to develop novel techniques to localizing short-circuit faults in power distribution networks accurately and efficiently.

In the next section, a brief introduction to the power distribution networks is presented. It is followed by a discussion about various types of faults observed in the distribution networks, together with their consequences and factors affecting their behavior such as the X/R ratio of the system.

1.2 Background Information

Before diving in detail into the topic of fault localization, it is important to understand the structure of the Power System. Traditionally, a power System is broadly divided into three parts: Power Generation, Power Transmission and Power Distribution. Electric power distribution is the portion of the power delivery infrastructure that takes the electricity from the high-voltage transmission circuits and delivers it to customers. Primary distribution lines are "medium-voltage" circuits, and have the voltage between 600 V to 35 kV. At a distribution substation, a substation transformer steps down the incoming transmission- level voltage (35 to 230 kV) and feeds several distribution primary circuits, which fan out from the substation. A feeder is an electrical distribution circuit fed from a single source point (breaker or fuse) at the substation. It operates at the primary distribution voltage and disseminates power through a portion of the substation's assigned service area which is its feeder service area [7]. Close to each end user, a distribution transformer takes the primary-distribution voltage and steps it down to a low-voltage secondary circuit (commonly 120/240 V). From the distribution transformer, the secondary distribution circuits connect to the end user where the connection is made at the service entrance. Figure 1.2 shows an overview of the power generation and delivery

3

infrastructure. Functionally, distribution circuits are those that feed customers. Figure 1.3(a) shows the North American Distribution Layout. [1]. Figure 1.3(b) shows a simple distribution system.
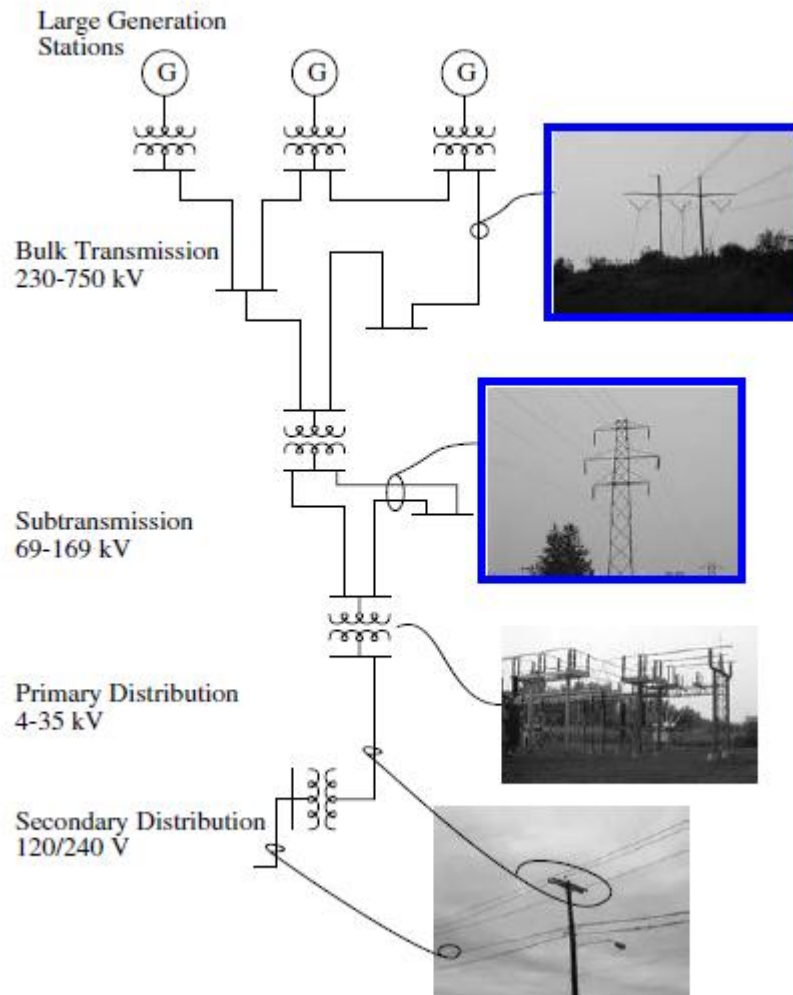
Figure 1.2 Overview of the Electricity Infrastructure [1]
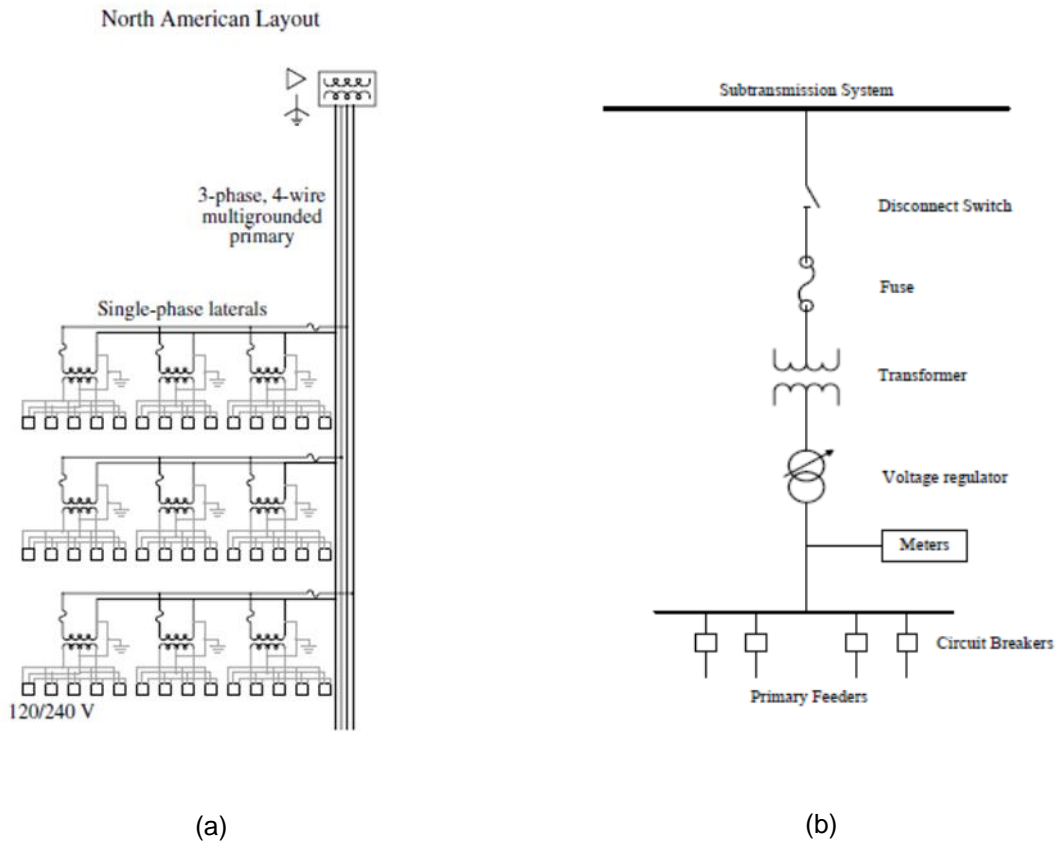
Figure 1.3 Distribution System Layout (a) North American Distribution Layout [1] (b) A simple distribution system

A single three phase transformer or three units of single phase transformers connected in a standard fashion are used in the distribution substation. The standard primary distribution voltage levels in common practice are 34.5 kV, 23.9 kV, 14.4 kV, 13.8 kV, and 12.47 kV [8] [9].

1.2.1 Different Types of Feeders and Distribution Systems

Voltage regulation, flexibility, security of supply, efficiency and cost are the major factors that measure the effectiveness of the distribution system. There are several basic types of feeders and feeder systems which include:

1.2.1.1 Radial Feeder

More than 80% of all distribution worldwide is accomplished using radial feeder systems, in which there is only one path between any customer and the substation (Figure 1.4, left) [7]. The radial distribution system generally feeds residential and non-commercial loads. Both low cost and simplicity of analysis and operation made radial systems popular in the beginning of the electric era, before computerization made analysis of complex circuit behavior reliable and inexpensive [1].

1.2.1.2 Loop / Ring Feeder

In case of loop feeder circuits the power flows into each "end" of a feeder and moves outward to customers (Figure 1.4, middle). The ring mains system is mostly used to supply bulk loads where service continuity is the major consideration. When built and protected properly, it can provide very high levels of customer reliability. Any equipment failure causes interruption to only a small group of customers [1].

1.2.1.3 Network / Grid System

Feeder networks consist of groups of feeders interconnected so that there is always more than one path between any two points in the feeder network (Figure 1.4, right). If designed with sufficient capacity and protection throughout, a feeder network can provide very high levels of customer reliability: the loss of any segment or source will not interrupt the flow of power to

any customers, and multiple failures can occur with little or no interruption [1]. The Figure 1.4 shows all these three types of distribution systems:
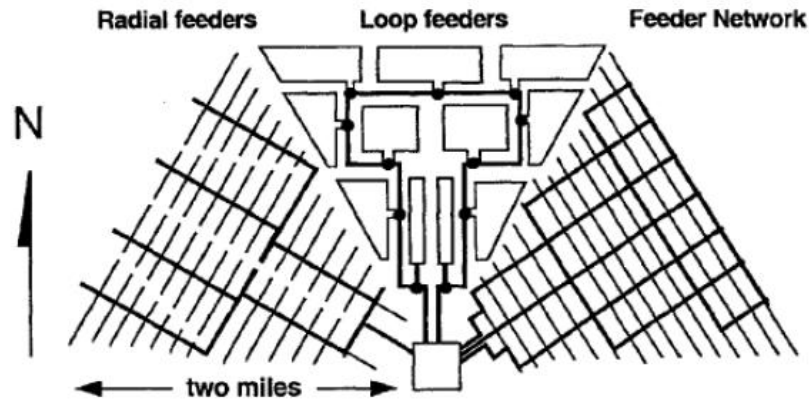
Figure 1.4 Different types of Distribution System [7]

The distribution system design varies according to different parameters including maximum load, load density, rural or urban area and type of loads (single or three phase, residential or industrial) and is an area of expertise on its own. The Distribution system can be classified in two types based on the physical location of cables inside or outside the ground: Overhead and Underground System. The Table 1.1 compares the advantages of these two systems:

Aesthetics is the main driver towards underground circuits. Especially in residential areas, parks, wildlife areas, and scenic areas, visual impact is important. Underground circuits are more reliable. Overhead circuits typically fault about 90 times/100 mi/year; underground circuits fail less than 10 times/ 100 mi/year. Because overhead circuits have more faults, they cause more voltage sags, more momentary interruptions, and more long-duration interruptions. Even accounting for the fact that most overhead faults are temporary, overhead circuits have more permanent faults that lead to long-duration circuit interruptions. The one disadvantage of

underground circuits is that when they do fail, finding the failure is harder, and fixing the damage or replacing the equipment takes longer. [1]

Table 1.1 Overhead vs. Underground Distribution [1]

Overhead vs. Underground: Advantages of Each

Overhead	Underground
Cost — Overhead's number one advantage. Significantly less cost, especially initial cost.	*Aesthetics* — Underground's number one advantage. Much less visual clutter.
Longer life — 30 to 50 years vs. 20 to 40 for new underground works.	*Safety* — Less chance for public contact.
Reliability — Shorter outage durations because of faster fault finding and faster repair.	*Reliability* — Significantly fewer short and long-duration interruptions.
Loading — Overhead circuits can more readily withstand overloads.	*O&M* — Notably lower maintenance costs (no tree trimming).
	Longer reach — Less voltage drop because reactance is lower.

The next subsection talks about the faults and their consequences in the power distribution network and in particular the underground network.

1.2.2 Faults in the Power Distribution Network

There are different types of faults on distribution circuits. A large EPRI study was done to characterize distribution faults in the 1980s at 13 utilities monitoring 50 feeders (Burke and Lawrence, 1984; EPRI 1209-1, 1983). The distribution of permanent fault causes found in the EPRI study is shown in Figure 1.5. It can be seen that Single-phase faults are the most common. Almost 80% of the faults measured involved only one phase either in contact with the neutral or with ground [10]. Most faults are single phase because most of the overall length of distribution lines is single phase, so any fault on single-phase sections would only involve one phase. Also, on three-phase sections, many types of faults tend to occur from phase to ground.

Faults are either temporary or permanent. A permanent fault is one where permanent damage is done to the system. This includes insulator failures, broken wires, or failed equipment such as transformers or capacitors.
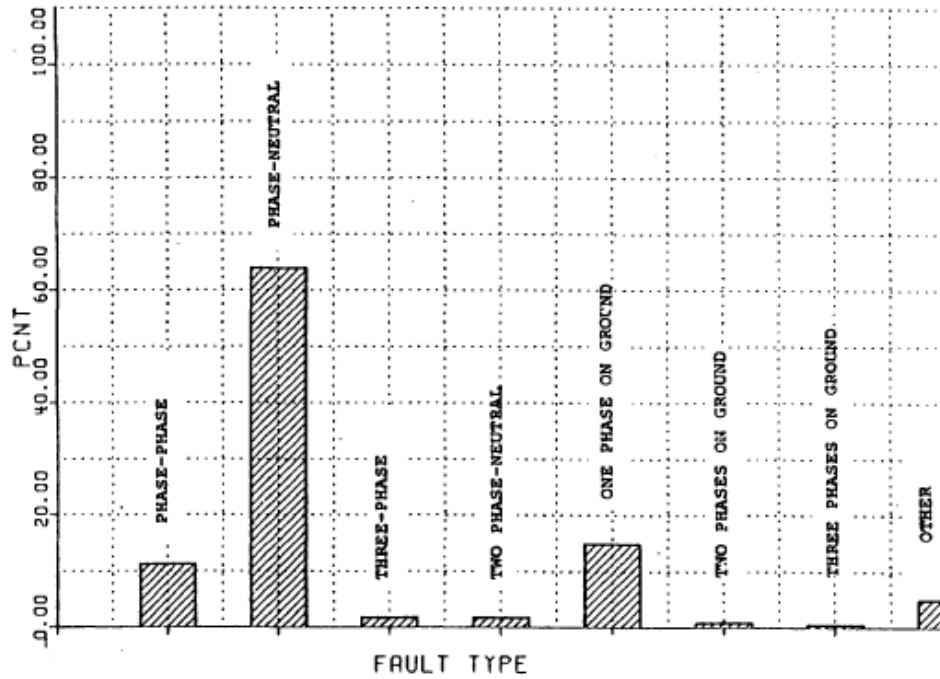
Figure 1.5 Different Types of Faults in the Distribution system [10]

Virtually all faults on underground equipment are permanent. Most equipment fails to a short circuit. Permanent faults on distribution circuits usually cause sustained interruptions for some customers. A permanent fault also causes voltage sag to customers on the feeder and on adjacent feeders. A temporary fault does not permanently damage any system equipment. If the circuit is interrupted and then reclosed after a delay, the system operates normally. Temporary (non-damage) faults make up 50 to 90% of faults on overhead distribution systems [1]

When there is a short-circuit fault in the network, the magnitude of fault current is limited only by the system impedance and any fault impedance. The system impedance includes the impedances of wires, cables, and transformers back to the source. For faults involving ground,

9

the impedance includes paths through the earth and through the neutral wire. In circuits containing resistance and inductance, it is possible to develop an initial fault current transient that exceeds the peak steady-state fault current. The resulting asymmetry in fault current, termed the dc offset, is dependent upon two factors [10]:

1.   The point on the voltage waveform where the fault is initiated

2.   The X/R ratio of the distribution circuit from the point of fault.

In general, the short circuit current is given by [1]:

$$i(t) = \sqrt{2}\, I_{rms} \sin(2\pi f t + \beta - \theta) - \sqrt{2}\, I_{rms} \sin(\beta - \theta)\, e^{-\frac{2\pi f t}{X/R}}$$

Where

$i(t)$ is the instantaneous value of current at time t

I_{rms} is the root-mean square (rms) value of the ac component of current

β is the closing angle which defines the point on the waveform at which the fault is initiated

θ is the system impedance angle = $tan^{-1}(\frac{X}{R})$

f is the system frequency, Hz

t is the time, sec

The decaying DC component depends on the X/R ratio. Usually, in the distribution system, X/R ratios of around 2 – 3 are found [10]:. Hence it can be seen that to accurately determine the fault current or voltage, it is required to have a filter which can filter out only the ac component.

In the next subsection, the methods used to determine the location of the fault used or proposed before are summarized. Here, the emphasis is given to the underground distribution network since most of the faults in the underground network are permanent and it is difficult to access all points in the network.

<u>1.3 Pertinent Literature and Present Practices for the Fault Localization</u>

The basic idea of locating fault in the distribution is based on the idea of the impedance seen from the source side. It is the same principle on which the Impedance relay is designed. While the idea is simple, a useful implementation is more difficult. Different fault types are possible (phase-to-phase, phase-to-ground, etc.), and each type of fault sees a different impedance. Fault currents may have offsets. The fault may add impedance. There are uncertainties in the impedances, especially the ground return path. Conductor size changes also make location more difficult [1]. These methods are subject to errors caused by high resistance ground fault, circuit topology, and interconnection to multiple sources.

In the case of Underground networks, utilities typically use the Faulted circuit indicators (FCIs). FCIs are used to detect faults on primary underground residential distribution (URD) circuits and are not expected to detect faults on the secondary side of padmounted transformers. They are shown in Figure 1.6. FCIs can be visualized as consisting of three basic components. The components are the sensor, the logic circuit, and the display. [11]
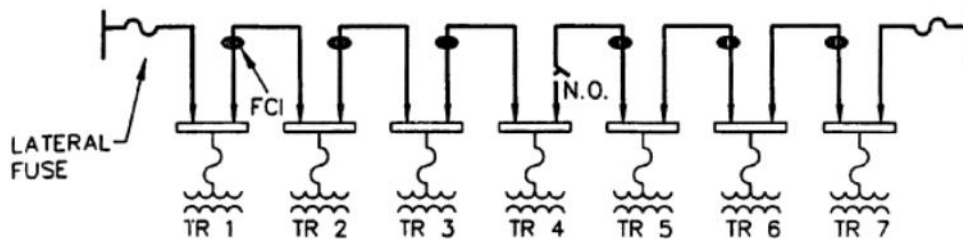
Figure 1.6 Faulted Circuit Indicators (FCIs) [11]

Faulted circuit indicators do not pinpoint the fault; they identify the fault to a cable section. After identifying the failed section, crews must use another method such as the

thumper to precisely identify the fault. Faulted circuit indicators can significantly decrease the fault-finding stage relative to the divide-and-conquer method.

There are other Off-line methods as well including the Section Testing where Crews isolate a section of cable and apply a dc hi-pot voltage. If the cable holds the hi-pot voltage, crews proceed to the next section and repeat until finding a cable that cannot hold the hi-pot voltage. Other off-line methods include a Thumper which is nothing but the application of a DC pulse to the cable. At the fault, the thumper discharges sound like a thumping noise as the gap at the failure point repeatedly sparks over. Crews can find the fault by listening for the thumping noise. Also, Radar can be used to estimate the location of fault in the cable.

However, most of these methods are useful for the radial type of network and require the distribution transformer to be disconnected since they are Off-line methods which increases the interruption time. Hence research is driven by the need of on-line methods which can be used to locate the fault quickly and accurately. Due to the complexity of distribution network, automated fault locations utilizing data from real time measurement of the system have been proposed.

F. Han [12] discussed the fault location in power systems using sinusoidal steady state analysis, where the current and voltage are measured at sending end, and by solving the nonlinear parameter equation of transmission line [13]. Other impedance based fault-location methods for transmission and distribution systems have been proposed in [14], [15] and [16]. An extended impedance-based fault-location formulation for generalized distribution systems is presented in [1]. The proposed method uses only local voltages and currents as input data.

Fault location utilizing power quality data also has been proposed using the fact that at different locations, different voltage sag characteristics are seen. By identifying the patterns at different location, the location of fault can be determined In [18] , the possible fault locations is estimated by incorporating the measured voltage sags magnitude and its corresponding phase angle into an equation of voltage sag as a function of fault distance. A ranking procedure is also

introduced to rank possible fault locations due the same electrical distance. Some more methods are summarized in [15]

In recent years, temperature sensors have been proposed to monitor cable faults [19] and power distribution equipment [20]. For example, Electric Power Research Institute (EPRI) used to execute a program named "Dynamic Thermal Capacity Rating (DTCR)." Several utility companies implemented similar pilot programs as well; for instance, Electric Reliability Council of Texas (ERCOT) initiated a SCADA program in 2007. A major drawback pertinent to using temperature sensors for fault detection is the relatively long lag time; due to the temperature sensors being very slow [21] to react to impedance faults and low intensity arcing faults [20]. Typical response time is around 1 second [21]. In addition, temperature sensors have to reside in the proximity of the fault locations to achieve sufficient sensitivity. Embedding these temperature sensors for fault inspection in large-scale underground networks would require numerous sensors densely distributed throughout the entire network, which is logistically demanding and cost prohibitive. There are also attempts to apply fiber optic sensors for the purpose of cable monitoring [23]. However several years ago, an investigation conducted by Con Edison concluded fiber optic sensors an ineffective solution, because of cost and effectiveness (probability of detection and false alarm rates) Other short-circuit fault locating techniques can be found in well-known textbooks [25][26][27].

1.4 Study Objectives

The research was motivated from the fact that in the power distribution network it is necessary to locate the fault quickly so as to reduce the interruption delay and increase the reliability of the system. The research was supported by Signal Processing Inc (SPI). This research was aimed towards building a solid framework to analyze the application of new methods directed towards localization of short circuit faults. The study objectives can be summarized as follows:

- It is necessary to test the proposed algorithms on the real world data. Hence, a build generic testbed setup which can be used to construct different circuits emulating different power distribution network configurations.

- Model the elements on the testbed so that they can be used in the simulations

- Start with a Radial or Serial network to understand the short circuit behavior by using simulations. Perform the analysis and try to investigate a method to localize the short circuit fault precisely on a feeder by using as few voltage and current measurements as possible.

- Focus the research on the analysis of a Mesh network configuration. Try to find an accurate and low cost method to localize the short circuit fault in a Network/ Mesh structure of feeders and distribution.

- Investigate more than one methods are compare the performance of these methods on the real world data by performing extensive experiments on the testbed

- Attempt to make the proposed algorithms cost effective by reducing the number of voltage or current inputs and analyze the performance of the methods.

1.5 Synopses of Chapters

The material in this dissertation is organized as follows:

Chapter 1 illustrates the importance of the localization of faults in the power system, introduces the general background of the distribution network and faults in the network and objective of this research.

Chapter 2 explains the hardware testbed setup built in the ESRC lab used to build different circuit configurations. It explains the procedure to make sure the absence of mutual inductances among the components and obtaining the modeling parameters for the components.

Chapter 3 talks about the procedures proposed to locate short circuit faults in the Serial distribution network. It is divided into two sections, one for the localization of dead short circuit (zero impedance faults) and the second deals with impedance faults. In both the sections, first a theoretical explanation of the procedure is given which is followed by experimental

Chapter 4 deals with the localization of faults in the Mesh Distribution network. In the first subsection, different hardware testbed built in the ESRC lab are explained along with the waveform measurement method. In the next section, detailed theoretical explanation of the two proposed methods is provided. The subsequent section deals with the results obtained from the application of both the methods on the measurements from the short circuit experiments.

Finally in Chapter 5, a summary of the research work is documented and it also discusses the opportunity for further research.

CHAPTER 2

HARDWARE TESTBED SETUP

In a realistic power distribution network, power is dispatched from the feeder to loads through lengthy and complex transmission lines. A testbed was built which constitute a matrix formation of coils (inductors) as shown in Figure 2.1. Over a 2" X 2" wooden board, a matrix of inductors was deployed and they were connected in different ways to emulate different realistic power distribution networks. The inductors are of cylindrical shape, with diameter 2.5 cm and height 2.5 cm.
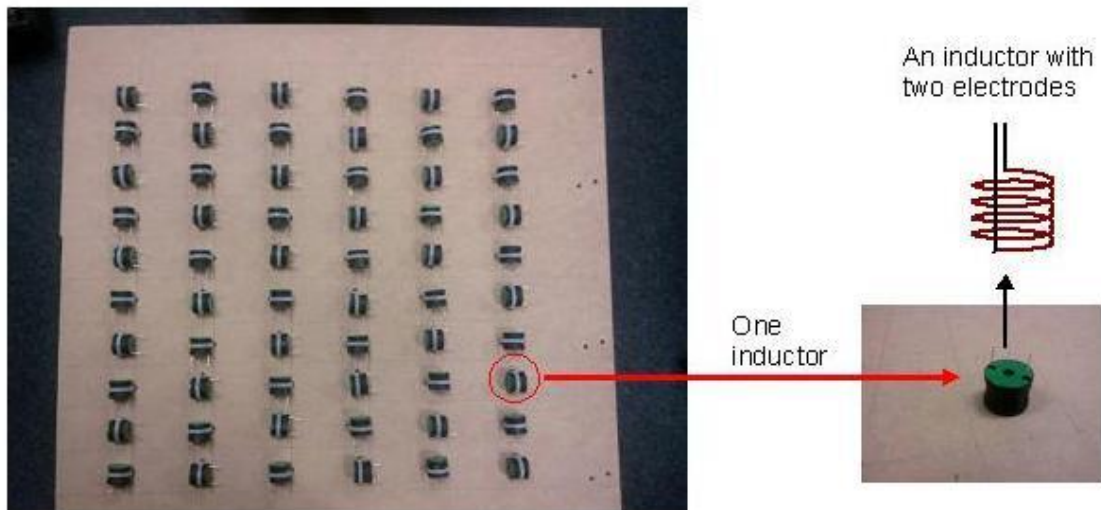
Figure 2.1 Matrix formation of coils (inductors) on the wooden board

Usage of inductors enables emulating a large-sized distribution network by a small test board. However at the same time, it may bring up a problem. If the inductors are placed too close to one another, their inductive couplings might be too strong. Since such mutual couplings

do not exist in realistic power distribution networks, they would prevent our testbed from precisely emulating the reality. Hence, it is critical to avoid the mutual coupling among inductors in our testbed. There are two methods to reduce the mutual coupling between two inductors. The first is to make their orientations misaligned, and the second is to enlarge the distance between them. In the testbed, both methods have been applied. As shown in Figure 2.1, every two neighboring inductors were perpendicular to each other; and, the separation among the inductors was large enough. Before this configuration was constructed, extensive measurements had been conducted to ensure all the mutual couplings among inductors were negligible. The measurement procedure and measurement results are presented in section 2.1. After making sure that the coils were weakly coupled next task of determining the impedance of the coil is explained in section 2.2.

2.1 Procedure To Determine Mutual Coupling

The measurement setup for mutual coupling is illustrated by two photos in Figure 2.2. Two inductors were placed with various separations and orientations. They were connected to a signal source and an oscilloscope, respectively. The signal source generated a continuous wave at a certain frequency, and the induced signal was read from the oscilloscope's screen.
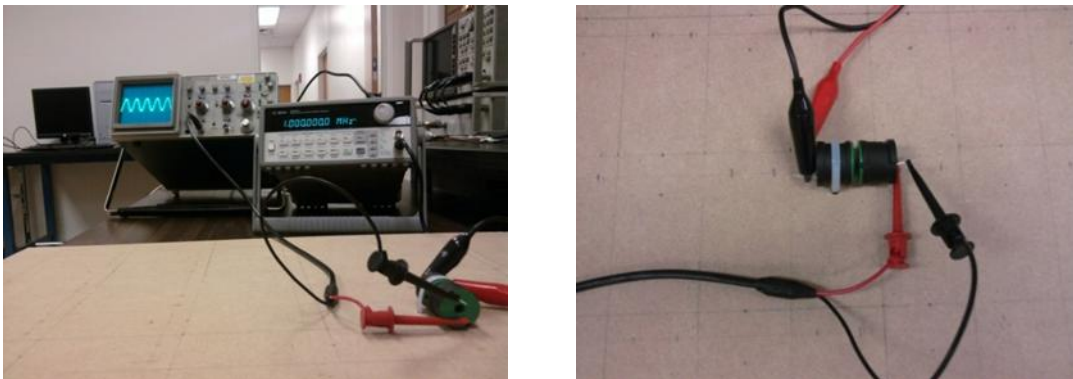
Figure 2.2 Illustration of the measurement setup for mutual coupling between two inductors

2.1.1 Experimental Measurements

Some of the measurements are summarized in Table 2.1. In the table, a square box with two pins is used to embody an inductor; and the two pins represent the inductor's two electrodes. The inductor connected to the signal source is marked by gray color and the inductor connected the oscilloscope marked with blue color is termed as the "the second inductor." The signal source generates sinusoidal wave with peak-to-peak (p-p) amplitude 1 V at various frequencies.

Table 2.1 Mutual Inductance Testing Measurements
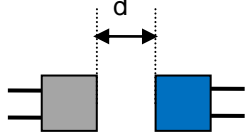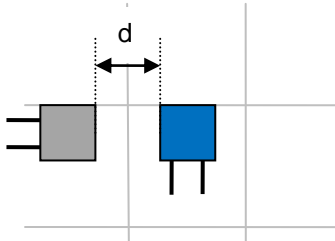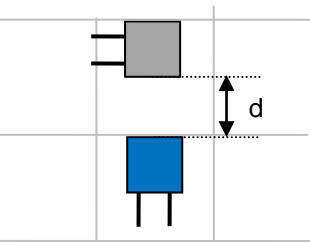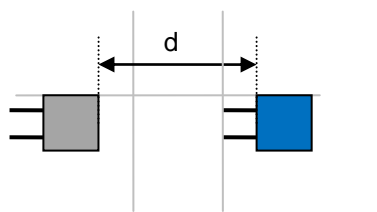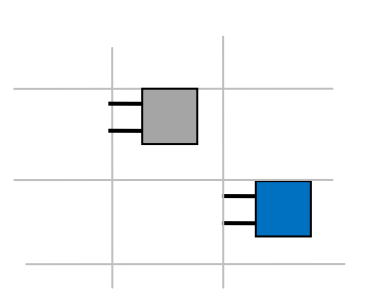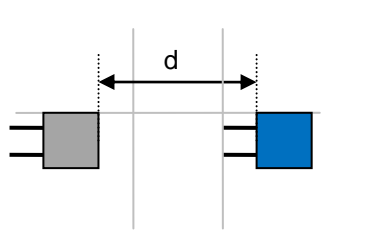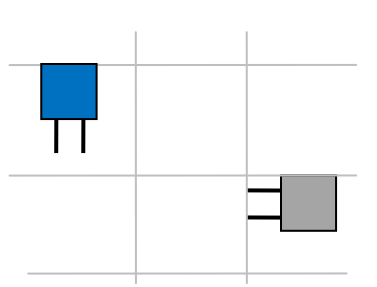
Case	Configuration	Distances	Signal to the 1st inductor		Voltage measured at the 2nd inductor
			Amplitude	Frequency	
1		d = 4 mm	1 V p-p	1 MHz	250 mV p-p
			1 V p-p	700 Hz	30 mV p-p
			1 V p-p	420 Hz	20 mV p-p
			1 V p-p	180 Hz	12 mV p-p
			1 V p-p	120Hz	10 mV p-p
			1 V p-p	60 Hz	Noise signal
2		d = 2.7 cm	1 V p-p	1 MHz	20 mV p-p
			1 V p-p	700 Hz	Noise signal
			1 V p-p	420 Hz	Noise signal
			1 V p-p	120 Hz	Noise signal
			1 V p-p	60Hz	Noise signal
3		d=7.5 cm	1 V p-p	1 MHz	15mV p-p (very weak)
			1 V p-p	700 Hz	Noise signal
			1 V p-p	420 Hz	Noise signal
			1 V p-p	120 Hz	Noise signal
			1 V p-p	60Hz	Noise signal

Table 2.1– *Continued*

4		d= 8cm	1 V p-p	1 MHz	15mV p-p (very weak)
			1 V p-p	420 Hz	Noise signal
			1 V p-p	120 Hz	Noise signal
			1 V p-p	60Hz	Noise signal
5			1 V p-p	1 MHz	Noise signal
			1 V p-p	420 Hz	Noise signal
			1 V p-p	180 Hz	Noise signal
			1 V p-p	180 Hz	Noise signal
			1 V p-p	60Hz	Noise signal
6		d=12.5cm	1 V p-p	1 MHz	Noise signal
			1 V p-p	420 Hz	Noise signal
			1 V p-p	120 Hz	Noise signal
			1 V p-p	60Hz	Noise signal
7			1 V p-p	1 MHz	Noise signal
			1 V p-p	420 Hz	Noise signal
			1 V p-p	120 Hz	Noise signal
			1 V p-p	60Hz	Noise signal

From the data in the above table, some observations are articulated below.

(i) In Case 1, the two inductors have aligned orientations and are 4 mm apart. The coupling is very strong at 1 MHz: the induced voltage is 1/4 as the source voltage. With the decrease of frequency, the coupling gets weaker. When the frequency is 60 Hz, only noise signal can be detected at the second inductor's terminal.

(ii) On the basis of (i), if the two inductors are misaligned or further separated, the coupling always gets weaker, which is as expected. Some small couplings are detected only when the frequency is as high as 1 MHz.

(iii) Cases 2 to 7 in the table represent the geometrical locations of inductors in the testbed. Clearly, when the frequency 60 Hz, their couplings are all negligible.

A testbed was built in which a matrix of inductors (coils) was deployed over a wooden board and they could be electrically connected to emulate realistic power distribution networks. Extensive measurements showed that the mutual coupling among inductors in the testbed was negligible for frequencies power frequency of 60 Hz. In the research, this testbed has been used to create circuits emulating different configurations of power distribution network.

2.2 Evaluating the impedance of the inductors connected in the network

The testbed included the coils which were used as building blocks for different circuit combinations. For the purpose of fault localization, it is necessary that the algorithm contains exact network model. To build the exact model, it is required to know the impedances of all the elements in the circuit. The inductors connected in the circuit; referred to as Cell Element in the diagram; are not ideal inductors and hence it consists of inductive part as well as resistive part. The values of inductance for the cells were measured using a digital multimeter and are found to be in the range of [0.557 mH, 0.663 mH]. However, the resistance value could not be measured accurately using the multimeter and hence an experiment was performed to find the value of the impedance of each cell element.

In order to measure the inductive reactance and resistance of each element, it was assumed that these values were more or less constant for all the elements in the circuit. This assumption was valid since the inductors used in the circuit were of the same model and same manufacturer.

Our testbed is illustrated in Figure 2.3. It consists of multiple cells serially connected. Each cell is implemented by a coil. Each coil can be modeled as a resistor together with an inductor. This serial network was excited by a power supply oscillating at 60 Hz. Quantities were measured in Figure 1: V_{in} and I_{in}. Specifically, V_{in} is the input voltage before the first cell and I_{in} is the current along the serial network. Both V_{in} and I_{in} are measured by an oscilloscope with the supplied power source as the reference. As a result, both of them are obtained as complex phasors.
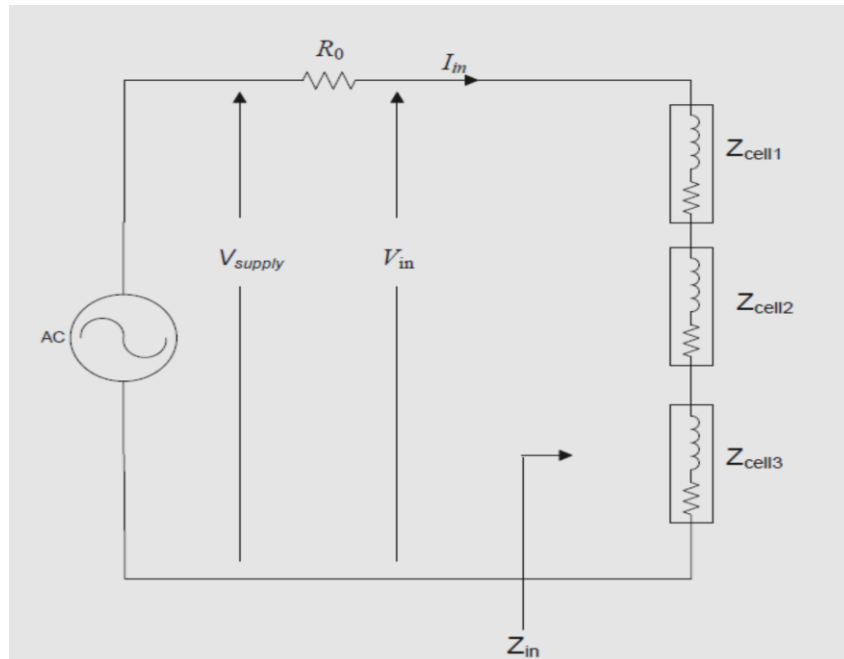
Figure 2.3 Measurement of the impedance of the coil

Since the oscilloscope is unable to measure the current I_{in} directly, the following indirect method is adopted. A probe resistor R_0 (with $R_0 = 1.57\Omega$ precisely known) is inserted before Cell 1, the voltages at R_0's two terminals (V_{supply} and V_{in}) are measured, the voltage drop across the probe resistor can be calculated then, and finally I_{in} is obtained by dividing the voltage drop by R_0.

$$I_{in} = \frac{V_{supply} - V_{in}}{R_0} \qquad (1)$$

It is to be noted here that while calculating above both V_{supply} and V_{in} are used as vectors. The relative phase angle between these quantities is calculated by measuring the time delay on the oscilloscope

This current also equals the ratio of voltage V_{in} and the impedance as seen from input ports marked as Zin in the diagram.

$$Zin = \frac{V_{in}}{I_{in}} \qquad (2)$$

For the case in the Figure 2.3where 3 cells connected in series, the impedance:

$$\therefore Zcell = \frac{V_{in}}{3I_{in}} \qquad (3)$$

In general, when we have 'n' cell elements in series connected to the power supply, using the same procedure, we can calculate the impedance of the cell elements as:

$$Zcell = \frac{V_{in}}{n\,I_{in}} \qquad (4)$$

The number of coils (cell elements) is varied from 1 to 5. For each case, the impedance of the cell is calculated. Table 2.2 provides the details of the readings recorded. Finally, an average of all the values is evaluated and is used henceforth for simulation and modeling purposes.

In this chapter, an effort made to verify the mutual coupling among the components in the testbed and to determine the modeling parameter values such as inductance and resistance of the coils are summarized. The next chapter elucidates method used in the localization of short circuit fault in a Serial or Radial network.

Table 2.2 Measurements to Determine the Impedance of Each Cell

Number of Inductors Connected	Voltage applied V_{supply}	Voltage after the resistance V_{in}	The quantity which is leading between V_{supply} and V_{in}	Time difference in ms	Phase difference in deg	Ru in ohms	Xu in ohms
1	0.37	0.06	V_{in}	2.13	46.008	0.1716	0.23179
2	0.4086	0.112	V_{in}	1.875	40.5	0.1589	0.2122
3	0.4534	0.179	V_{in}	1.56	33.696	0.1811	0.2297
4	0.501	0.2435	V_{in}	1.45	31.32	0.1634	0.244
5	0.55	0.3	V_{in}	1.21	26.136	0.18	0.237

The average value of the impedance of the cell was $Zcell$ = 0.17 + j0.23 ohms

In reality, various fluctuations could occur in the power distribution networks and these fluctuations are hard to estimate. It is a general

practice to model the power distribution networks using average values. Therefore, our assumption emulates realistic scenarios.

CHAPTER 3

SERIAL DISTRIBUTION NETWORK

In the case of a serial network, when a short circuit fault occurs at any point, the voltage at the sending end changes due to increase in the current. The receiving end voltage also gets affected due to presence of a short in the line. In this research, this fact has been used to localize the fault. Mainly, two types of short circuit faults are considered:

1.   Solid Short Circuit (Zero Impedance) Fault: In this case, the voltage at the fault point is zero. In the case of distribution network

2.   Impedance Faults: These faults have non-zero impedance between the fault point and the ground. Also, the voltage at the fault point is not zero. Although not with zero impedance, "impedance" faults are as harmful as "short" faults since they may cause excessive current flows as "short" faults do.

In the ESRC lab, a testbed was built emulating a serial distribution network using the setup with the coils mentioned in the last chapter. A number of tests were conducted and the algorithm for the localization of short circuit fault was tested on the data collected from the experiments. The next two sections explain the experimental setup, measurements and localization scheme in detail for both types of faults.

<div align="center">3.1 Localization of Solid Short Circuit Fault</div>

3.1.1 Experimental Hardware Testbed

The testbed is illustrated in Figure 3.1. It consists of 40 cells serially cascaded. Each cell is implemented by a coil. Each coil can be modeled as a resistor together with an inductor as mentioned in the Chapter 2. This serial network was excited by a power supply oscillating at 60 Hz. A "zero impedance" or "short" fault was introduced artificially at various locations in the serial network by connecting that point to ground; and here the objective was to find the fault location.
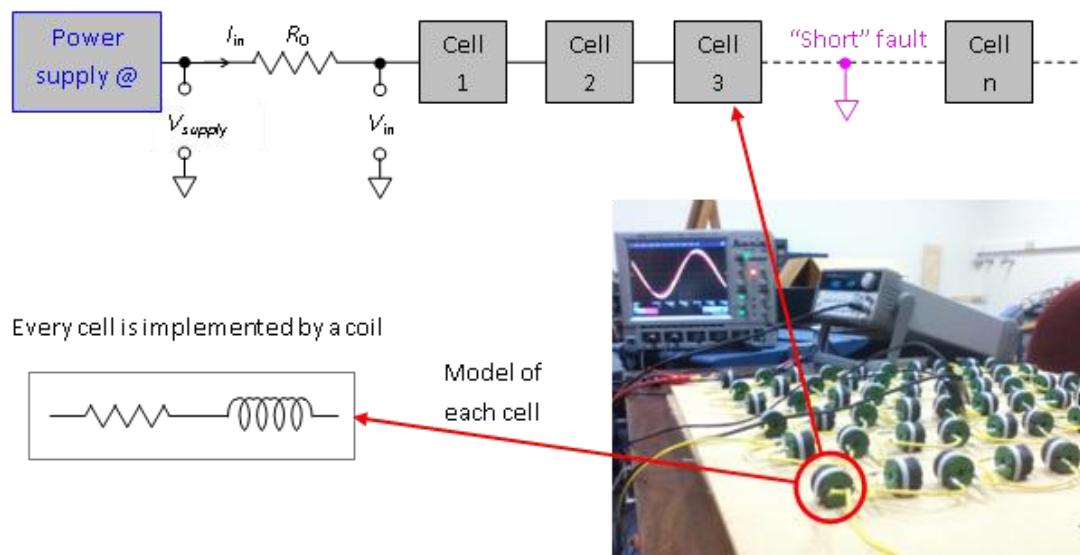
<div align="center">Figure 3.1 Illustration of our experimental testbed</div>

In order to localize the "short" fault, two quantities were measured in Figure 3.1 V_{in} and I_{in}. Specifically, V_{in} was the input voltage before the first cell and I_{in} was the current along the serial network. Both V_{in} and I_{in} were measured by an oscilloscope with the supplied power source as the reference.

As a result, both of them were obtained as complex phasors. Since the oscilloscope was unable to measure the current I_{in} directly, the following indirect method was adopted. A

probe resistor R_0 (with $R_0 = 1.57\,\Omega$ precisely known) was inserted before Cell 1. The voltages at R_0's two terminals (V_{supply} and V_{in}) were measured, the voltage drop across the probe resistor can be calculated then, and finally I_{in} was obtained by dividing the voltage drop by R_0. Once V_{in} and I_{in} were measured, input impedance (with complex value) of the serial network was calculated as.

$$Z_{in} = \frac{V_{in}}{I_{in}} \tag{5}$$

It was assumed that all the cells in the serial networks have identical impedance Z_{cell}. Next, an integer value m was computed as

$$m = \left\lceil \frac{Z_{in}}{Z_{cell}} \right\rfloor \tag{6}$$

Where, the operator " $\lceil \ \rfloor$ " takes the integer closest to its argument. It was therefore estimated that there are m cells before the "short" fault. Each cell was assumed to have impedance $Z_{cell} = 0.17 + j0.23$ ohms at 60 Hz, with $j = \sqrt{-1}$. In reality, various fluctuations could occur in the power distribution networks and these fluctuations are hard to estimate. It is a general practice to model the power distribution networks using average values. Therefore, the assumption emulates realistic scenarios.

3.1.2 Measurements and Result

Some of our localization results are plotted in Figure 3.2. Results from 10 tests are presented. The test measurement data is listed in Table 3.1. In each test, a "short" fault was placed in the serial network. The horizontal axis of Figure 2 consists of the tests' indices; the vertical axis is m, the number of cells between the power supply and the "short" fault. As shown in Figure 2, the actual m value varies from 2 to 40. Generally, the fault location can be accurately found by our measurement technique. Out of 10 tests, 2 errors happen, in Test Number 5 and Test Number 8, respectively. For both errors, the estimated m value only

deviates from the actual m value by 1. It means that the measurement is capable of localizing the "zero impedance" fault reliably.

Table 3.1 Measurements for Localization of Zero Impedance Short Circuit Faults

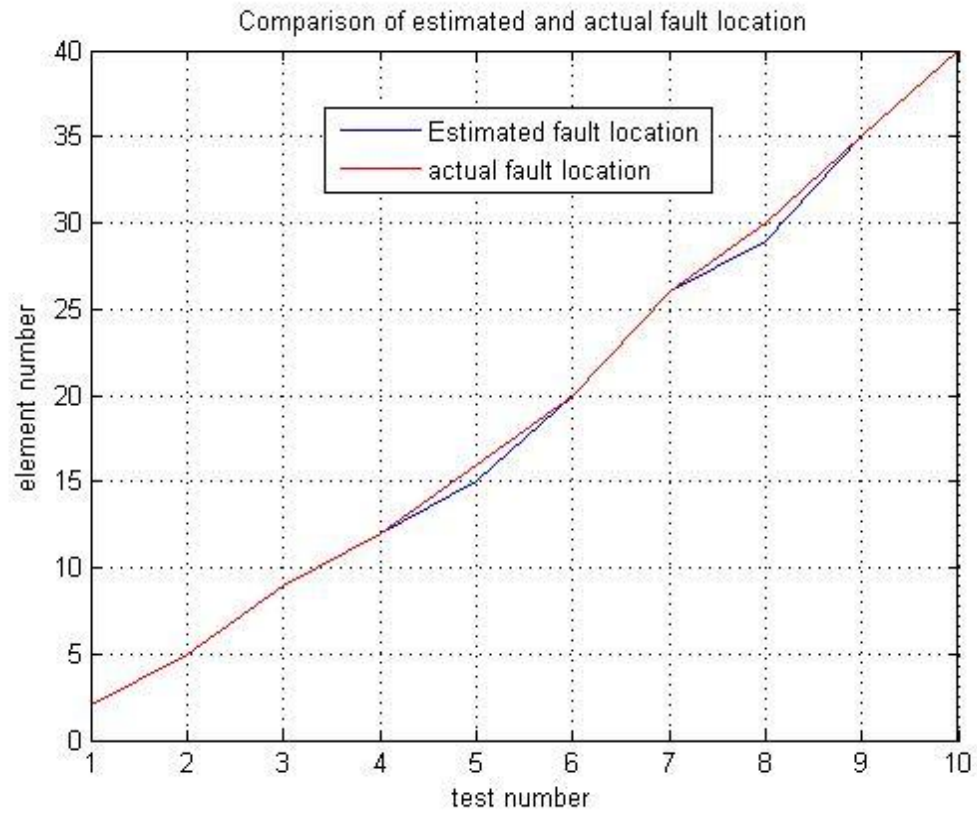| Resistance Rprobe in ohms	Number of Inductors Connected before the short point	Voltage applied V_{supply} in Volts	Voltage after the resistance V_{in} in Volts	Time difference in ms	The quantity which is leading between V_{supply} and V_{in}	Phase difference in deg
1.57	2	0.7	0.205	1.914	V_{in}	41.3424
1.57	5	0.926	0.49	1.358	V_{in}	29.3328
1.57	9	1.278	0.888	0.971	V_{in}	20.9736
1.57	12	1.526	1.16	0.787	V_{in}	16.9992
1.57	16	1.9	1.52	0.65	V_{in}	14.04
1.57	20	2.235	1.89	0.527	V_{in}	11.3832
1.57	26	2.745	2.415	0.424	V_{in}	9.1584
1.57	30	3.065	2.73	0.375	V_{in}	8.1
1.57	35	3.455	3.15	0.325	V_{in}	7.02
1.57	40	3.82	3.53	0.295	V_{in}	6.372

Figure 3.2 Results from the Localization of 'zero impedance fault'

<u>3.2 For The Impedance Faults</u>

3.2.1 Experimental Testbed

      The experimental testbed is depicted in Figure 3.3. Overall, it is the same as in the previous subsection; the only difference is that, the "short" fault in our previous report is replaced by a fault resistor to emulate "impedance" faults. The testbed consists of 40 cells serially cascaded. Each cell is implemented by a coil, with average impedance $Z_{cell} = 0.17 + j0.23$ ohms at 60 Hz, with $j = \overline{-1}$. This serial network is excited by an AC power supply at 60 Hz, and it is terminated by a load R_L. In our experiments, a resistor R_{fault} is used to emulate the "impedance" fault; its location is varied along the serial network and its value varies from 0.51 Ω to 3.08Ω.
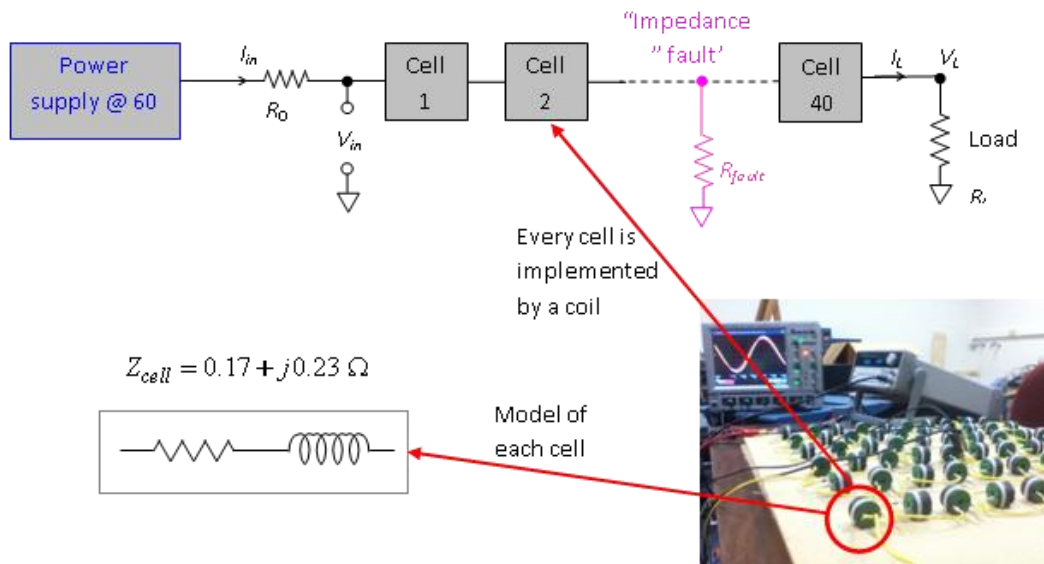

Figure 3.3 Illustration of the testbed

3.2.2 Localization Technique

In order to localize the impedance fault, measurements were conducted at both the power supply and the load: as illustrated in Figure 3.3, four values were measured: V_{in} , I_{in}, , V_L and I_L . Again, out of the four quantities, V_{in} and V_L were measured directly, while I_{in} and I_L were obtained through measuring the voltage drops across R_0 and R_L respectively as explained in the section 2.2.1

All the four measured quantities were complex phasors. However, their phases did not have a global reference. To be specific, when V_{in} and I_{in} were measured at the power supply. Their phases were with respect to a local phase reference; while V_L and I_L at the load had another local phase reference. This assumption is consistent with realistic scenarios: in reality, the power supply and load may be miles apart and it is practically difficult for them to share the same global phase reference.

After the four quantities were measured, two tracking curves were plotted, which termed "FORWARD TRACKING PROFILE" and "BACKWARD TRACKING PROFILE," respectively. The intersection point of the two profiles was used to estimate the fault location. The two profiles are explained in the following.

(a) Forward tracking is depicted in Figure 3.4. Starting from V_{in} and I_{in} , voltages along the serial network are calculated by assuming the fault does not exist.
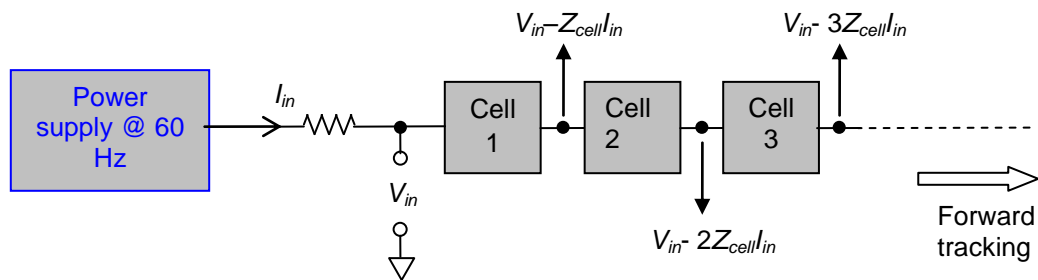

Figure 3.4 Illustration of Forward Tracking

(b) Backward tracking is depicted in Figure 3.5. Starting from V_L and I_L, voltages along the serial network are calculated by assuming the fault does not exist.
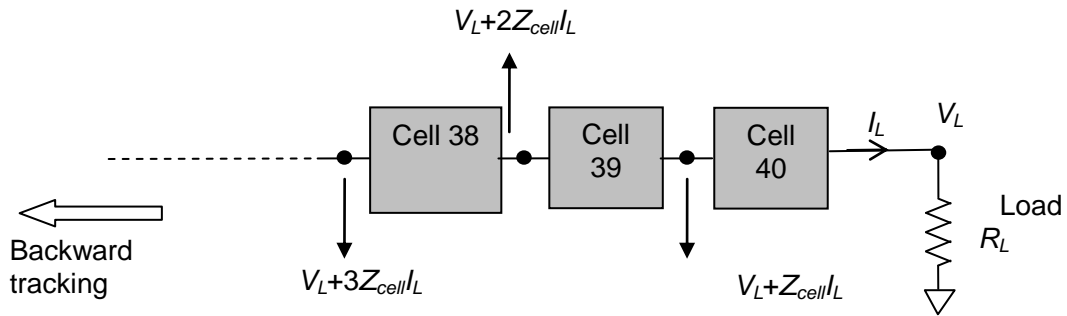

Figure 3.5 Illustration of Backward Tracking

Because there is no global phase reference, the phase information obtained from "Forward Tracking" and "Backward Tracking" is not used. In our processing, only the magnitude profiles are plotted for the two trackings, which result in "Forward Tracking Profile" and "Backward Tracking Profile."

When there is no fault (that is, the serial network stays in the normal state), the two profiles are identical to each other. The slope of both the voltage profiles will be small and they can be considered as flat profiles.

When there is an "impedance" fault in the radial network, the "forward tracking profile" and "backward tracking profile" differ from each other. In the case of a fault, current drawn by the fault i.e. the fault current is much bigger than the load current. Hence as is it done in all the short circuit studies, the load current is neglected. Since "Forward Tracking" is unaware of the current drawn by the fault, its profile is not a straight line any longer; instead, it decreases first and increase afterwards. The "Backward Tracking" profile stays as a straight line. This is because of the fact that when there is a fault on the line, the voltage at the end of the line is very small and the current drawn by the load is also very small compared to the fault current. This

can be achieved in simulation by using $R_L = \infty$. When the two profiles are plotted on top of each other, they may have two intersection points. The intersection point residing at the falling slop of the "forward tracking profile" is selected as the estimated fault location, since the rising slop in the "forward tracking profile" is not realistic.

In the experiments, all the cells were assumed to have impedance Z_{cell} , which was the average impedance among all the cells. In practice, the cells' realistic values may deviate from the average value. As a result, sometimes the two profiles do not intersect; in this case, the fault is estimated to be at the position where the two profiles have the minimum distance.

3.2.3 Localization Results

The localization results are presented in this section. In all the figures in this section, a vertical line in pink color denotes the actual location of the fault; and, the "Forward tracking curve" and "Backward tracking curve" are plotted to estimate the fault location.

The fault impedance R_{fault} was chosen to have three values: 0.51Ω, 1.59Ω, and 3.08Ω. For each resistance value, the fault impedance was placed at six locations (nodes in the serial network.
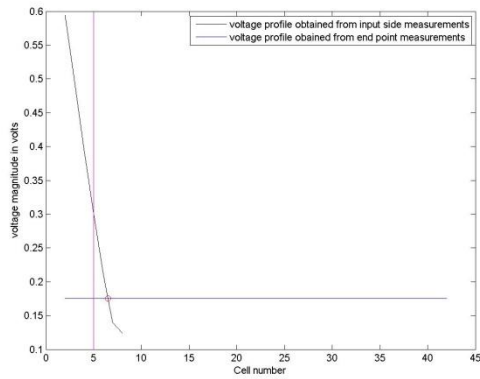
Results for $R_{fault} = 0.51 \, \Omega$, with six fault locations, are shown in Figure 3.6

Results for $R_{fault} = 1.59 \, \Omega$, with six fault locations, are shown in Figure 3.7
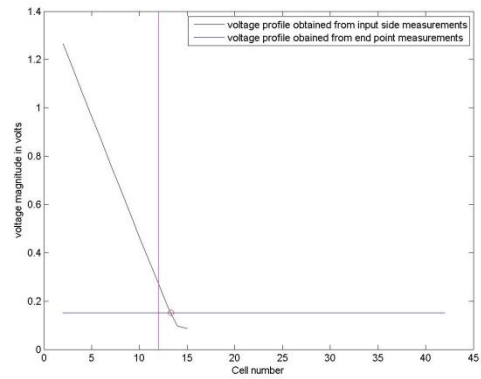
Results for $R_{fault} = 3.08 \, \Omega$, with six fault locations, are shown in Figure 3.8

In Figure 3.6 to Figure 3.8, a vertical line in pink color denotes the actual location of the fault; and, the "Forward Tracking Curve" and "Backward Tracking Curve" are plotted to estimate the fault location. Measurement data for Figure 3.6 to Figure 3.8 are listed in the Appendix A.

In the Figure 3.6 to Figure 3.8, fault locations are as follows: First location is node 2, Second location is node 4, Third location is node 6 Forth location is node 8 and Fifth location is node 13. All the results in Figure 3.6 to Figure 3.8are summarized in Figure 3.9. In Figure 3.9, the actual fault locations are compared to the locations estimated using our technique, for all the eighteen cases in Figure 3.6 to Figure 3.8 (there are three fault impedances and for each fault impedance, six fault locations are tested).

(a)

(b)
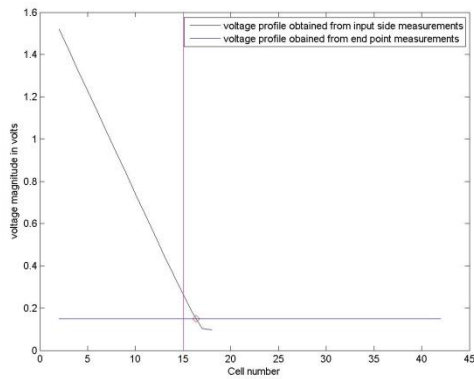
(c)
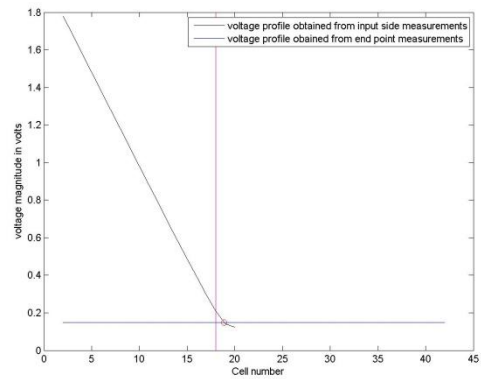
(d)
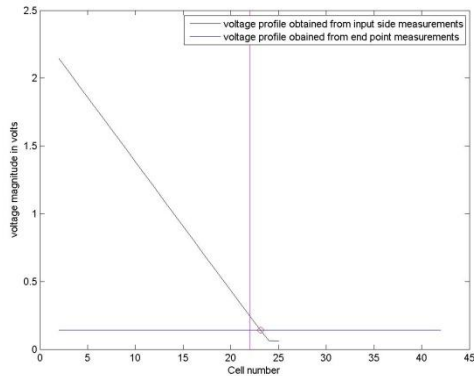
(e)
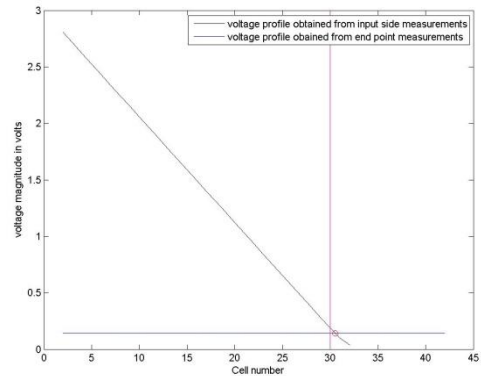
(f)

Figure 3.6 Fault localization results for $R_{fault} = 0.51\ \Omega$ (a) The first fault location (b) The second fault location (c) The third fault location (d) The fourth fault location (e) The fifth fault location (f) The sixth fault location

(a)

(b)

(c)
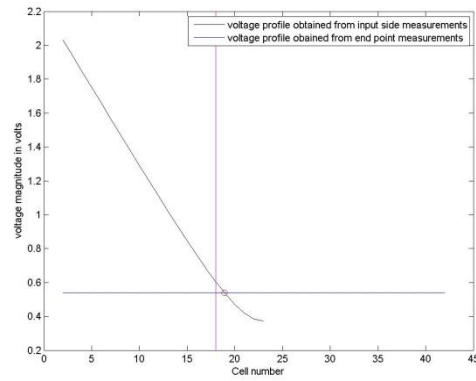
(d)
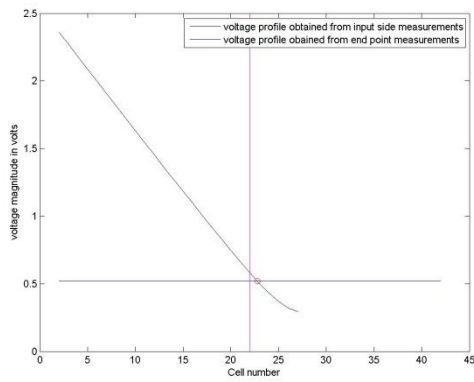
(e)
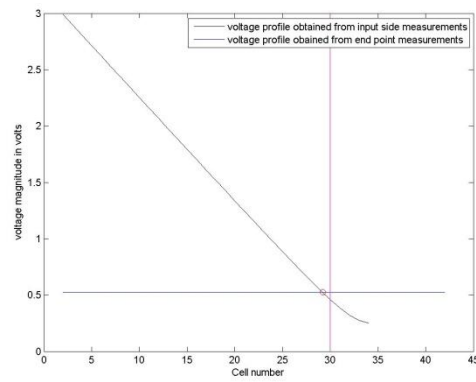
(f)

Figure 3.7 Fault localization results for $R_{fault} = 1.59\,\Omega$ (a) The first fault location (b) The second fault location (c) The third fault location (d) The fourth fault location (e) The fifth fault location (f) The sixth fault location
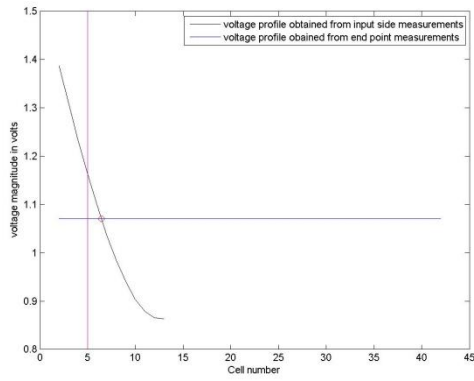
(a)
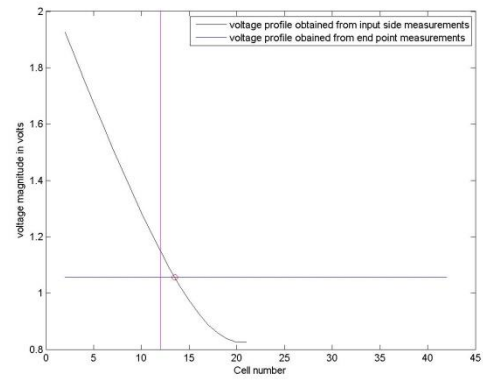
(b)
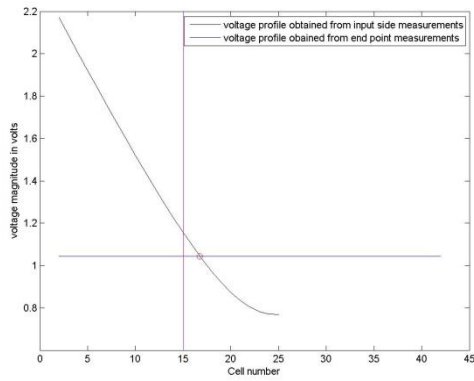
(c)
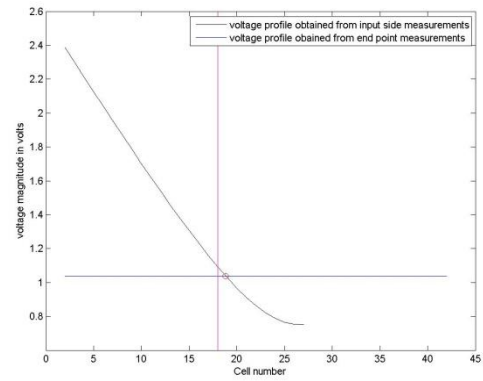
(d)
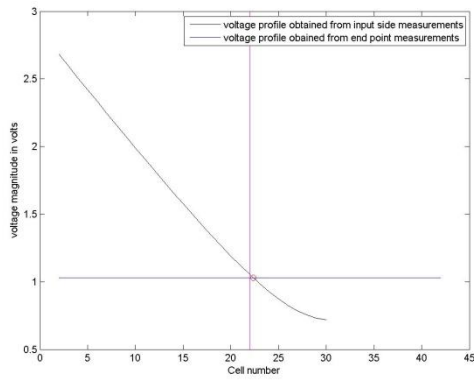
(e)
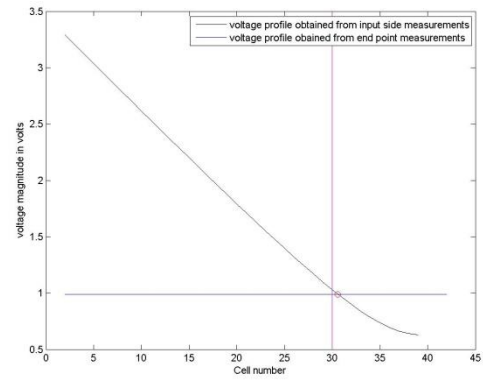
(f)

Figure 3.8 Fault localization results for $R_{fault} = 3.08\,\Omega$ (a) The first fault location (b) The second fault location (c) The third fault location (d) The fourth fault location (e) The fifth fault location (f) The sixth fault location
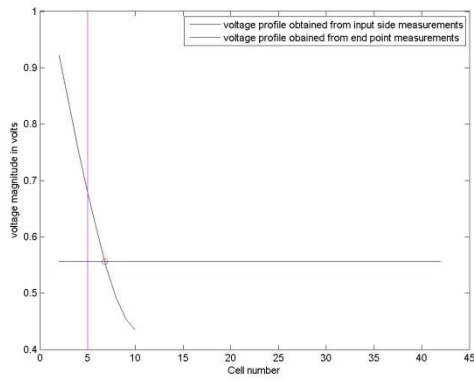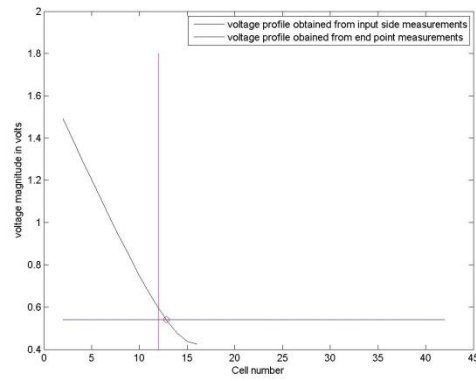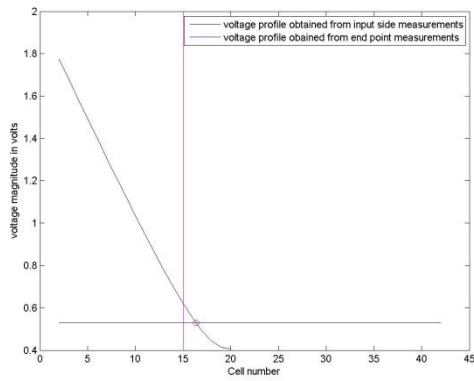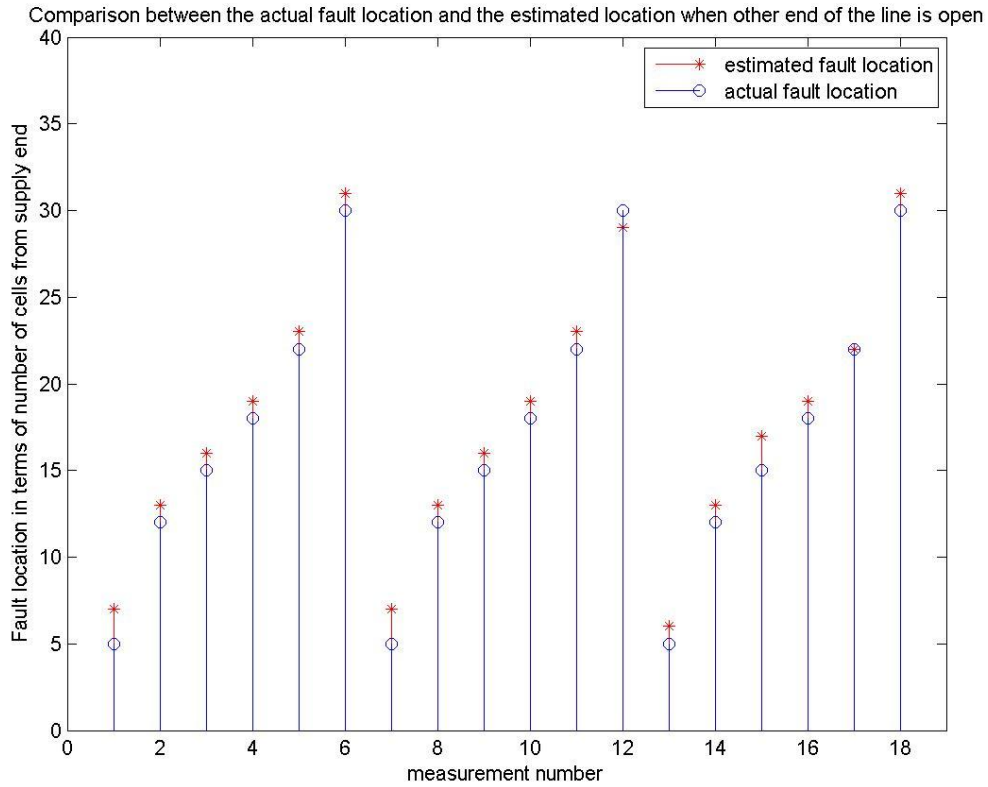
Figure 3.9 Comparison between actual fault locations and estimated fault locations for all the 18 experiments in Figure 3.6 to Figure 3.8

From Figure 3.9, it can be observed that the technique is capable of estimating the fault location accurately. First six measurements correspond to $R_{fault} = 0.51\Omega$, measurement numbers 6 to 12 correspond to $R_{fault} = 1.59\Omega$ and measurement numbers 13 to 18 correspond to $R_{fault} = 3.08\Omega$. In all the eighteen cases, the differences between the two sets of data (i.e., the estimated fault locations and the actual fault locations) were found to be at most three cells.

CHAPTER 4

MESH DISTRIBUTION NETWORK

Secondary grid networks are distribution systems that are used in most major cities. The secondary network is usually 208Y/120 V in the U.S. Five to ten primary distribution circuits (e.g., 12.47-kV circuits) feed the secondary network at multiple locations [1]. They are more complicated to analyze and operate than radial circuits [7].
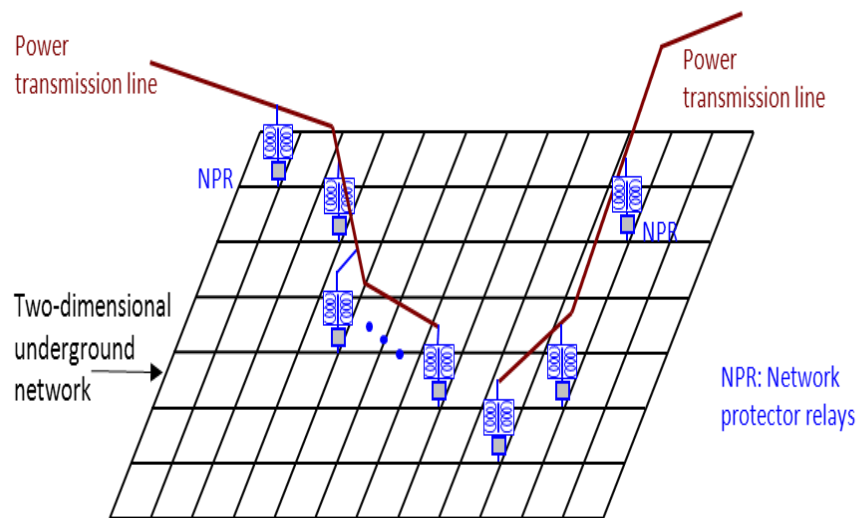
Figure 4.1 Representation of a Grid/Mesh Distribution Network

One such grid network could be seen in Con Edison's power system. Con Edison operates one of the most complex electric power systems in the world. It also maintains the

most reliable electric service in the world. In 2006, PA Consulting Group named Con Edison the most reliable electric utility for the northeast region. The system performs at a level that is seven times above the national average [28]. A part of the system is shown in Figure 4.2
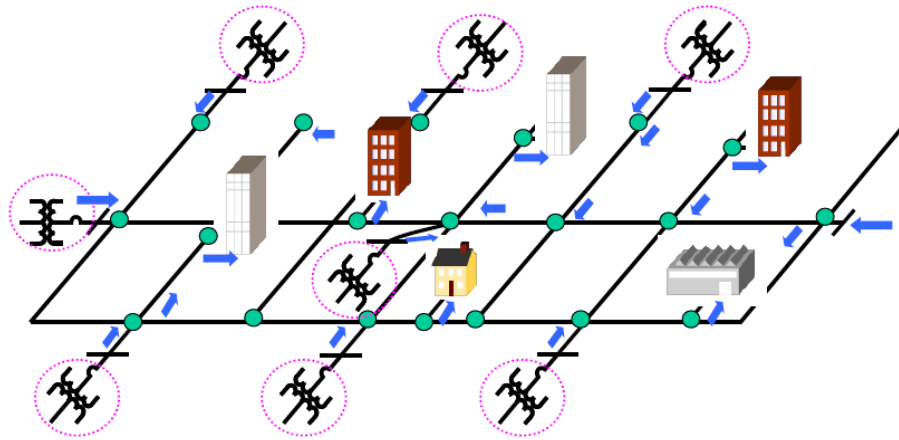
Figure 4.2 Example of Part of the Con Edison's Distribution Network [28]

In the following sections, first the different hardware testbed configurations built in the lab to test the algorithms are described. Then a thorough description of both the algorithms is provided. Finally, the fault localization results of the algorithms on the actual measurement data are provided.

In a mesh network each node may be connected to more than one node and hence there are many branches present. In the ESRC lab at UTA, two different power distribution circuits were built from the testbed setup described in Chapter 2. The two circuit configurations have different number of nodes and dimension in terms of the number of rows and columns present.

Figure 4.3 shows a photo of the actual testbed in the lab. Each coil can be modeled as "a resistance + an inductance," whose impedance at 60 Hz is $0.17 + j0.23\ \Omega$, with $j = \sqrt{-1}$ as determined in section 2.2.1.

Each coil can be modeled as "a resistor + an inductor"

$0.17 + j\,0.23\ \Omega$
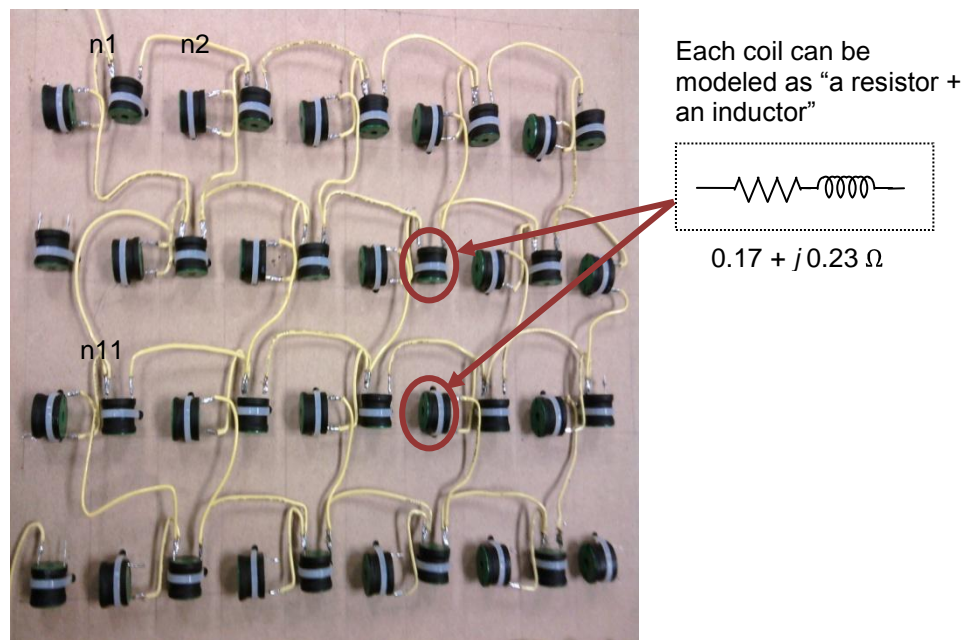
Figure 4.3 Photo of the testbed

4.1.1 Different Mesh Circuit Hardware Testbed Configurations

The two different configurations are explained below and the figures alongside represent the normal state of the network i.e. without any fault:

4.1.1.1 20 Nodes 4 x 5 Network

The coils are deployed in 4 rows and 5 columns. As illustrated in the equivalent circuit in Figure 4.4, there are altogether 20 *nodes* in the network, with indices n1, n2,… n20. A coil resides in between every two adjacent nodes and hence the impedance between any two directly connected nodes is same and equal to $Z_{cell} = 0.17 + j0.23$ Ω. This circuit is excited by a power supply oscillating at 60 Hz and connected between Node n1 and Node n20
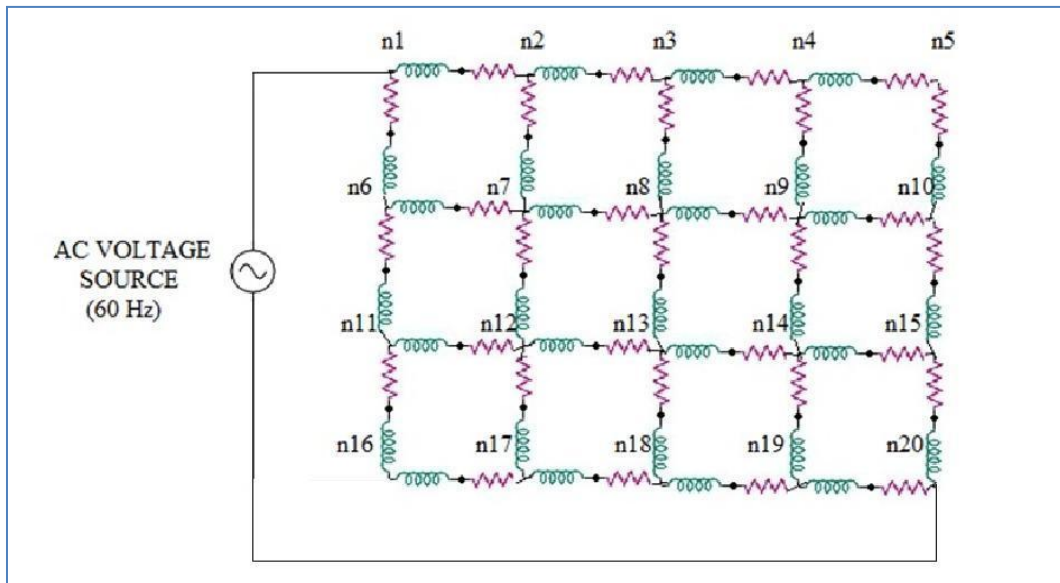
Figure 4.4 Circuit Diagram of 20 nodes 4 x 5 network

4.1.1.2 50 Nodes 10 x 5 Network

This time, the coils are deployed in 10 rows and 5 columns. As illustrated in the equivalent circuit in Figure 4.5 there are altogether 50 *nodes* in the network, with indices n1, n2, …,n50. A coil resides in between every two adjacent nodes and hence the impedance between any two directly connected nodes is same and equal to $Z_{cell} = 0.17 + j0.22$ Ω. This circuit is excited by a power supply oscillating at 60 Hz and connected between Node n1 and Node n50
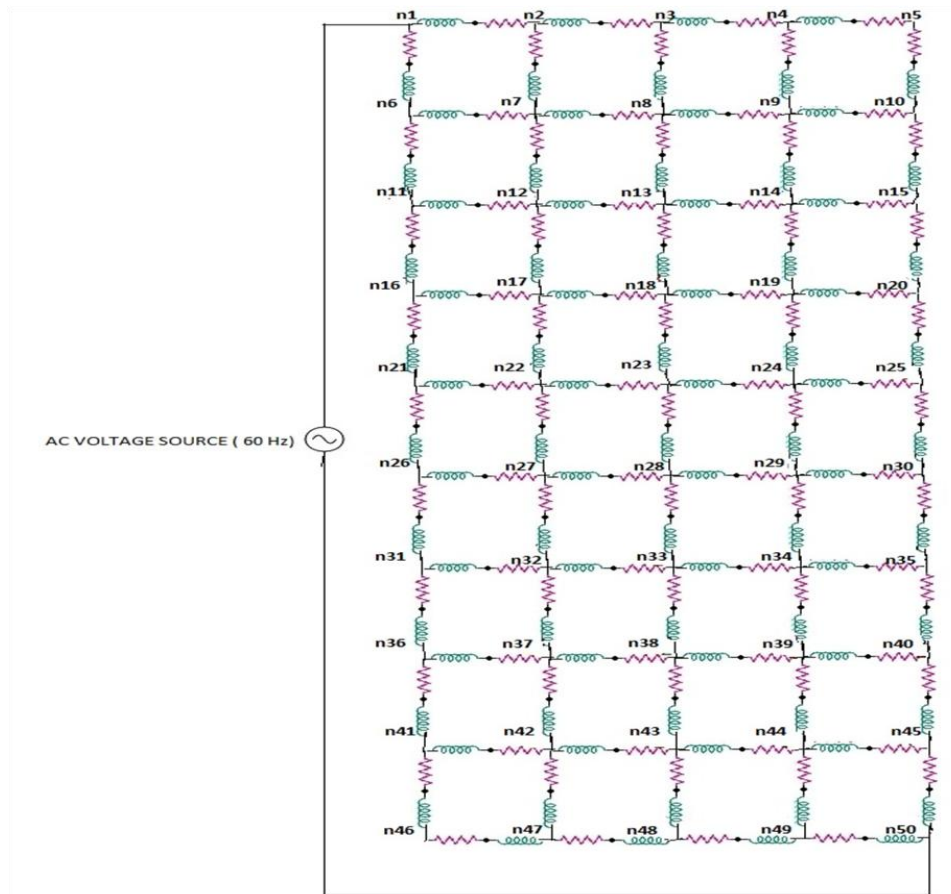
Figure 4.5 Circuit Diagram of 50 nodes 10 x 5 network

4.1.2 Waveform Voltage Measurement

In the ESRC lab, a digital storage oscilloscope was used to record the waveforms at all the nodes (with sampling frequency 1 MHz); and post-processing was conducted using Matlab to filter out the phasor at 60 Hz.

In the filtering algorithm, the concept of Fourier Transform was used. The Fourier transform of the signal is given by:

$$F(\omega) = \int_{-\infty}^{\infty} f(t)\, e^{-j\omega t}\, dt \qquad (7)$$

The formula is approximated for its use with the experimental data as follows:

$$F(\omega) \approx \sum_{n=-\infty}^{\infty} f(t_n)\, e^{-j\omega t_n} \Delta t \approx \sum_{n=0}^{N} f(t_n)\, e^{-j\omega t_n} \Delta t \qquad (8)$$

Where,

$f(t_n)$ is the sampled value of f(t) at $t = t_n$

$\omega = 2\pi f$ is the frequency at which the signal magnitude is required.

$\Delta t = \dfrac{1}{sampling\ frequency} = \dfrac{1}{10MHz}$ is the sampling time in sec.

N is the total number of samples recorded by the digital storage oscilloscope.

Frequency f = 60 Hz is put in the above equation. The magnitude of the result is calculated and multiplied by a scaling factor $(\dfrac{2}{N\Delta t})$ to get the magnitude of the fundamental (60 Hz) component from the sampled data. The scaling factor corresponds to the midpoint of the total time for which the voltage signal is recorded. It is the factor by which the amplitude spectrum is affected.

$$Fundamental\ (60Hz)\ voltage\ magnitude = abs\left(F(\omega)\right)_{\omega=2\pi*60} \times \frac{2}{N\Delta t}$$

This procedure emulates installing voltage sensors and microprocessors at individual nodes. The voltage magnitude calculated from the above method is used as the measured value of the voltage in the research.

<u>4.2 Fault Localization Schemes</u>

For the localization of short circuit faults in the Mesh distribution network, two algorithms have been developed with the help of Signal Processing Inc. (SPI). These algorithms are:

1.   SIGNATURE PATTERN RECOGNITION

2   SPARSE SENSING

For both the fault detection methods, it was necessary to simulate the distribution circuit in consideration for different fault conditions. The simulations were performed in SPICE and Simulink PowerSim Toolbox. The algorithms were implemented on the actual measured data from the tests performed on different circuit configurations. MATLAB was used to implement the algorithms on the experimental data. Signal Processing Inc (SPI) used MATLAB and C programming language to generate visually impressive results and evaluate the speed of the algorithm.

4.2.1 Signature Pattern Recognition

The idea is based on the signature recognition techniques used in the signature or image matching technique. First, a "pattern" is defined for the mesh network, which consists of voltage magnitudes at multiple nodes in the network. Second, a "library" of signatures is established through simulating the mesh network with all possible fault locations. Third, when a realistic fault is introduced in the mesh network, a pattern is obtained through measurement. Finally, fault localization is achieved by comparing the measured pattern to the simulated patterns in the library and identifying simulated pattern with the closest distance to the measured pattern. Figure 4.6 shows the concept of this pattern recognition method.
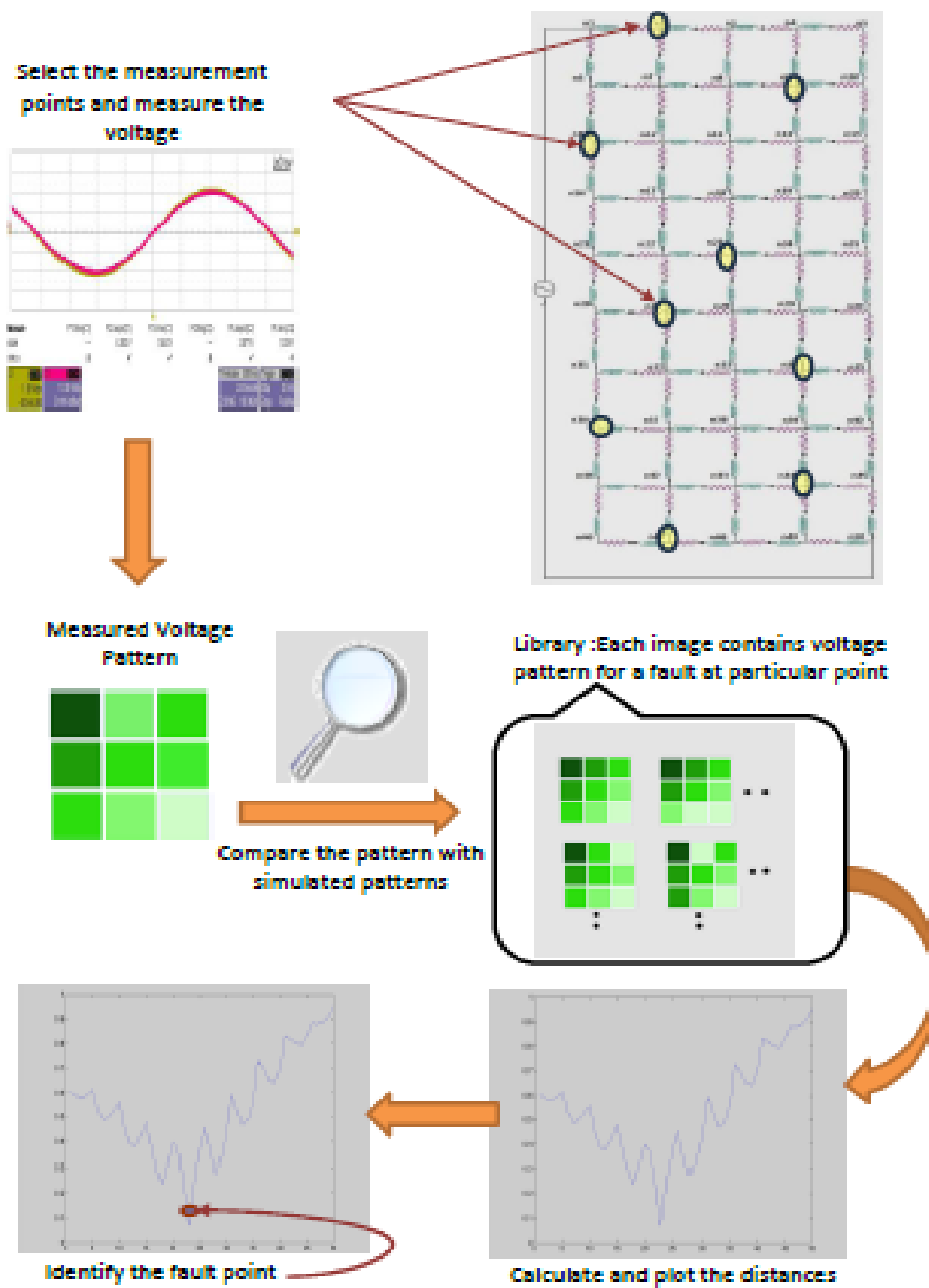
Figure 4.6 Signature Pattern Recognition

4.2.1.1 Mathematical Explanation

In order to facilitate fault localization, a *pattern* is defined for the "normal state" and every "abnormal state." The "normal state" is the state of the network when there is no fault present. When faults are introduced in the mesh network, "abnormal states" occur. In the experiments, "abnormal states" are obtained by connecting a certain node to the ground directly, i.e., by creating "short" faults

Consider a 'N' nodes mesh power distribution network where the nodes are denoted by $n_1, n_2 \dots n_N$. In general, a *pattern* consists of the voltage magnitudes at the 'R' nodes, and the 'R' voltage magnitudes are obtained through either simulation or measurement. It is clear that R≤ N and R is a subset of N.: Let the elements of R be $r_1, r_2 \dots r_R$.

To construct a pattern, voltage magnitudes at the 'R' nodes are collected and normalized by the maximum values among them. In this report, a pattern is denoted by a capital bold symbol, for instance, **P.** Mathematically, a pattern is a vector with 'R' elements

$$P = V_{r_1}, V_{r_2}, \dots V_{r_R} \tag{9}$$

Where $V_{r_1}, V_{r_2}, \dots V_{r_R}$ are the voltage magnitudes (after normalization) at nodes $r_1, r_2 \dots r_R$ respectively. Due to normalization, all the voltage values in a pattern are in the range of [0, 1].

Patterns can be generated through simulating the circuit. In the simulations, "short" fault is placed at all the 'N' nodes sequentially, and as a result, N patterns are yielded

$$S_1 \quad S_2 \quad S_3 \dots S_N$$

These 'N' patterns share symbol "S" as they are obtained from simulation. Their subscripts denote the corresponding fault locations. Because these 20 simulation patterns include all the possible fault locations, they are considered to constitute a "library."

Through the measurement we obtain a measured pattern M**.** The measurements are taken at the same 'R' nodes. Next, for every measured pattern, it is compared to all the simulated patterns in the "library." The simulated pattern with the closet distance to the measured pattern is "recognized" for the fault localization purpose. Performance of this pattern

recognition algorithm heavily relies on "how to define the distance between two patterns." In

this study, least square rule is used. Specifically, given two patterns

$$A = [\, A_1 \, A_2 \, A_3 \, ...\,... \, A_r \,]$$

$$B = [\, B_1 \, B_2 \, B_3 \, ...\,... \, B_r \,]$$

Their distance is evaluated as

$$d_{AB} = \sum_{k=0}^{r} |A_k - B_k|^2 \qquad\qquad (10)$$

The signature or the simulated pattern with the closet distance (with distance defined in

the least-square sense) to the realistic or the measured pattern is identified for purpose of fault

localization. In the analysis performed, to get the accurate results, first the voltage

measurements at all the nodes are used to form a "pattern". This means that R = N. It is clear

that this method gives the most accurate results as all the voltage information is used to find the

closest match.

4.2.1.2 Modification of the Localization Scheme

Ideally, this method can give us very accurate results if we measure voltages at all the

nodes to get the "pattern". This means that for the case where set R is equal to set N, we

should get accurate results. In real world circumstances, the implementation faces the following

problems:

- The measured signal contains noise which affects the voltage measurement

- The impedance information used in the simulations may not exactly match with the

    impedances in the actual circuit

- It is not possible to measure voltages at all the nodes every time

To overcome this, a small set of measurement data is used. Instead of measuring the voltages at all the nodes, the voltage measurement is performed at only a few selected nodes. This means that R <N. The key issue is the definition of "pattern," in other words, how to select of measurement nodes. The number of measurement nodes should be minimized without sacrificing the precision of fault localization. In this research, the effects of reducing the number of measurement points and hence using a smaller length pattern are studied. After running many simulations, it is found that the measurement nodes should be distributed evenly across the network. This is reasonable as one does not posse knowledge of the fault location

Signal Processing Inc (SPI) has suggested to use a strategy to select nodes based on some criteria, like feature selection. It is proposed to use a covariance based feature selection algorithm to automatically select certain number of top nodes using the dictionary data. Basically, a set of nodes which have maximum covariance is selected.

4.2.2 Sparse Sensing

4.2.2.1 Mathematical Explanation

This algorithm starts with standard circuit analysis for the power distribution network, yielding the following matrix equation

$$Z\,I = V \tag{11}$$

In, I and V are vectors with dimension m. Z is a square matrix with dimension $m \, x \, m$; where m is the number of nodes in the power distributions network (for instance, there are 50 nodes in the network in Figure 4.5. Vector V stores the voltages at all the nodes; each element of I stands for vector of the "total currents". The "total current" at a node is defined as the sum of all the currents at the branches connected to this node. According to Kirchhoff's Current Law (KCL), it is nothing but the current between the node and ground or source. Z is the impedance

49

matrix relating I to V which can be obtained by taking inverse of Y_{Bus} matrix for a given network.

It can be seen that, for an open node 'i' (not connected to generator or ground), corresponding ith element in the I vector equals to zero.

$$I_i = 0$$

If we know the injection node 'i' and the corresponding voltage v, the 'i'th element of:

$$V_i = v$$

While constructing the Y_{Bus} matrix, we use the following convention:

Let m i contains the neighborhood nodes of node i. For non-injection node,

$$Y_{ii} = \sum_{k \in m \ i} \frac{1}{z_{ik}} \quad , Y_{ik} = \frac{1}{z_{ik}} \quad for \ i, k \in m$$

For injection node,

$$Y_{ii} = 1 \text{ and } I_i = 1$$

Other elements of Y_{Bus} are zeros.

Next, a "reduced-set" matrix equation is derived from (11):

$$Z_0 I = V_0 \qquad\qquad (12)$$

In the above equation, V_0 is a vector with dimension c, where c is the number of measurement nodes (that is, nodes at which voltages are measured); and, V_0 contains the c measured voltages. Correspondingly, Z_0 is a matrix with dimension $c \ x \ m$, and, it is obtained by keeping c rows of Z. The vector I is still of the length m, corresponding to actual number of nodes present.

Most elements in vector I are zeros. An element of I is non-zero only in two cases. The first case is for "injection nodes," at which the actual power sources inject current into the network; in this project, it is assumed that all the injection nodes are known. The second case is

50

for "fault nodes," at which the nodes are connected to the ground with small impedances. As a result, after the injection nodes are excluded, the non-zero elements in I correspond to fault nodes. In the rest of this algorithm, the objective is to identify non-zero elements in I with minimal c. After defining

$$I' = I - I_p \tag{13}$$

Where I_p includes currents at all the injection nodes. Substituting for I in the equation (12)

$$Z_0(I' + I_p) = V_0$$

$$\therefore Z_0 I' + Z_0 I_p = V_0$$

$$\therefore Z_0 I' + Z_0 I_p = V_0$$

$$\therefore Z_0 I' = V_0 - Z_0 I_p \tag{14}$$

$$\therefore \quad Z_0 I' = V_0' \tag{15}$$

Where

$$V_0' = V_0 - Z_0 I_p \tag{16}$$

The number of non-zero elements in I' is identical to the number of fault nodes. Then, vector I' is solved for via (15) by a least-square solver, with the constraint that there are only a small number of non-zero elements in I'. In this implementation, the constraint is enforced by letting a certain combination of elements be non-zero and exhausting all the possible combinations. For every combination, I' is solved for and residue $Z_0 I' - V_0'{}_2$ is found. Finally, the combination with the smallest residue value is selected as the fault nodes.

4.3 Fault Localization Results

The schemes explained in section 4.2 are tested on the hardware mesh circuit configurations built in the ESRC lab. The fault localization results in the case of a Mesh distribution network are summarized in this section. Firstly, the results of fault localization using Signature Pattern Recognition are presented and effect of reducing the number of measurement points is discussed. Secondly, the results of fault localization using Sparse Sensing method are presented.

4.3.1 Signature Pattern Recognition
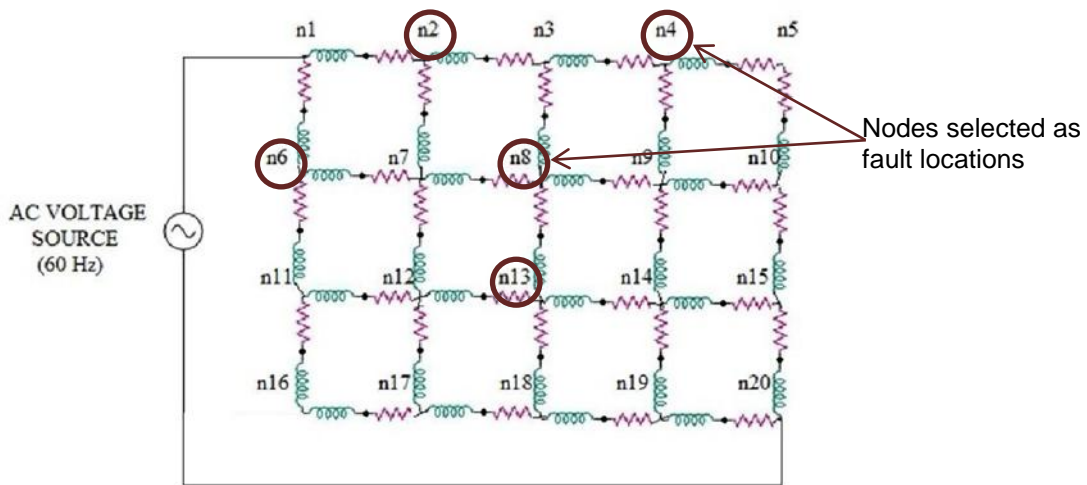
4.3.1.1 20 Nodes 4 x 5 Network

Figure 4.7 20 Nodes 4 x 5 Network

For this circuit configuration, 5 locations were chosen for the "short" faults, which were Nodes n2, n4, n6, n8, and n13. These are shown in the above Figure 4.1. For these 5 "abnormal states", 5 patterns were measured Hence five realistic measured patterns are generated, with corresponds to actual short-circuit locations at 2, 4, 6, 8, and 13, respectively

$$M_2 \ M_4 \ M_6 \ M_8 \ M_{13}$$

These measured patterns are listed in Table 4.1.In order to apply the signature pattern recognition algorithm (described in section 4.2.1); a signature dictionary was constructed by simulating the circuit in Figure 4.7 with all the 20 possible fault locations.
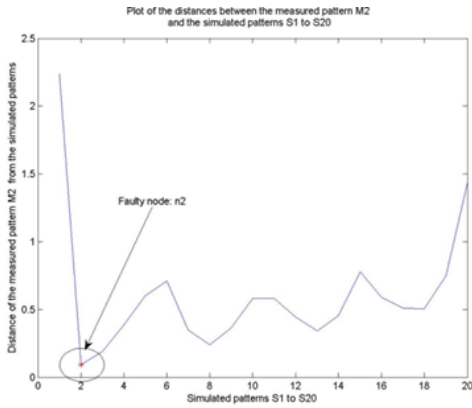
Table 4.1 Measured Patterns in the 20 Node Network

Node Number	The normalized measured voltages for the fault in the circuit at node 'm'				
	M_2	M_4	M_6	M_8	M_{13}
1	1	1	1	1	1
2	0.1557	0.6173	0.5563	0.5478	0.6150
3	0.1828	0.3377	0.3818	0.2719	0.3981
4	0.1761	0.0691	0.2807	0.1838	0.2858
5	0.1621	0.0955	0.2362	0.1586	0.2386
6	0.5689	0.6800	0.1552	0.6021	0.6238
7	0.3027	0.5167	0.2953	0.3856	0.4552
8	0.2216	0.3337	0.2797	0.0963	0.2849
9	0.1812	0.1750	0.2395	0.1333	0.2222
10	0.1563	0.1260	0.2097	0.1289	0.1921
11	0.4076	0.5281	0.1878	0.4275	0.4230
12	0.3029	0.4412	0.2235	0.3227	0.3008
13	0.2277	0.3150	0.2191	0.1836	0.0878
14	0.1695	0.1931	0.1883	0.1314	0.1285
15	0.1081	0.1134	0.1506	0.0970	0.1145
16	0.3168	0.4622	0.1902	0.3547	0.3389
17	0.2831	0.4006	0.2006	0.2921	0.2620
18	0.2186	0.2945	0.1870	0.1979	0.1460
19	0.1465	0.1660	0.1431	0.1203	0.1011
20	0.0516	0.0278	0.0523	0.0330	0.0297

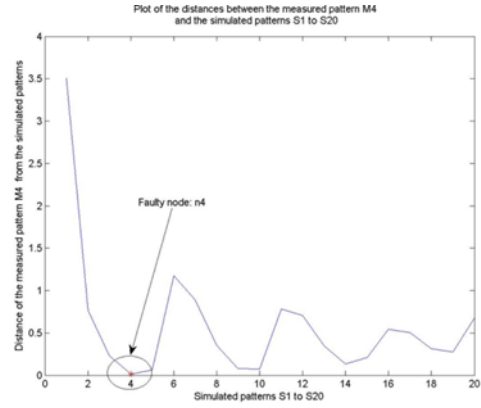**Signature Pattern Recognition Results by Using a Measured Pattern of 20 Elements**

Here all the node voltages (node n1 , n2…n20) are selected to form the "pattern". Hence each measured and simulated pattern is of length 20. It is clear that in this case N=R=20. As discussed in the section 4.2.1, for every measured pattern, it is compared to all the simulated patterns in the "library." The comparison results are plotted in Figure 4.8. In each diagram, the horizontal axis is the index of the 20 signatures and the vertical axis is the distance to the realistic measured pattern. The simulated pattern with the closet distance to the measured pattern is "recognized" for the fault localization purpose.

In the plot (a) of Figure 4.8 , it is clear that S_2 has the smallest distance to M_2. Hence, Node 2 is correctly identified as the fault location. The above is repeated for the other four measured patterns (corresponding to actual short-circuit locations at 4, 6, 8, and 13, respectively). For all the five measured patterns, the fault locations are identified precisely.
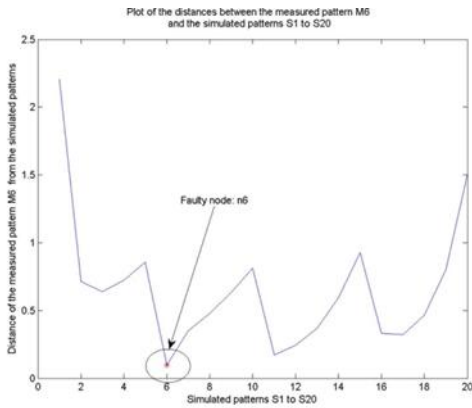
Ideally the distance between M_2.and S_2 should be zero, whereas in practice it is not. The major discrepancy between simulation and measurement is that, our simulation assumes impedance value $0.17 + j0.23 \, \Omega$ for every coil while the practical impedance values exhibit certain fluctuations which change the voltage values in the real world
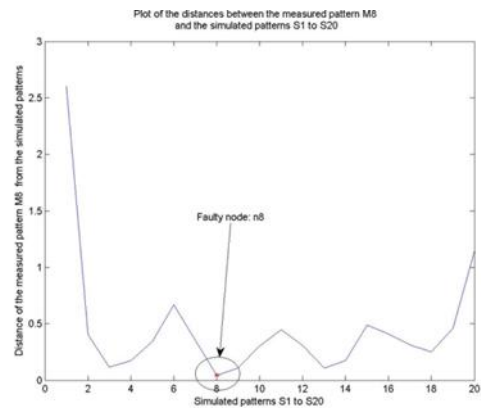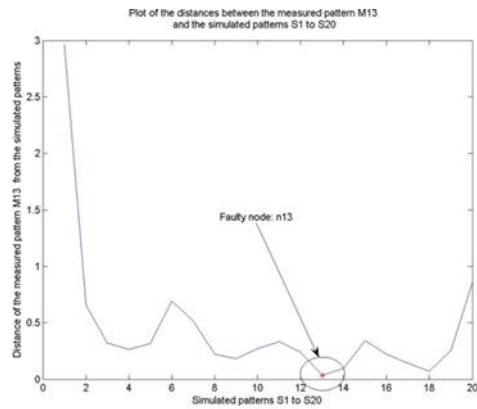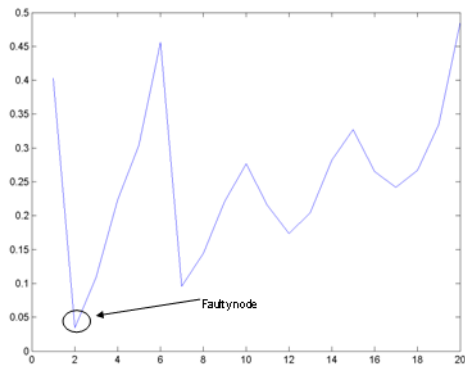
Figure 4.8 Distances between the Measured Pattern (of 20 elements) and the Simulated Patterns in the 20 nodes network (a) Actual short-circuit fault at Node 2 (b) Actual short-circuit fault at Node 4 (c) Actual short-circuit fault at Node 6 (d) Actual short-circuit fault at Node 8 (e) Actual short-circuit fault at Node 13

Signature Pattern Recognition Results by Using a Measured Pattern of Only 4 Elements

As explained in the section 4.2.1.2, a few measurement points are chosen to form the "pattern". Four measurement nodes are selected: Nodes 2, 5, 6, and 14. In this case, N = 20 and R = 4. Then, each measured pattern consists of four elements, that is, voltages at Nodes 2, 5, 6, and 14. Also the simulated pattern is consists of four elements which are voltages obtained from simulation at the same nodes 2, 5, 6 and 14.

Again, the simulated pattern with the closet distance to the measured pattern is "recognized" for the fault localization purpose. The comparison results are plotted in Figure 4.9. For all the five measured patterns, the fault locations are identified precisely.

The key to this modification is the selection of the nodes which will be the part of the pattern. From the experiments it is found that measurement nodes should be distributed evenly across the network. It is noted that, in some cases the second minimal distance is close to the minimal value, which may cause mistaken localization in practice. This potential risk can be relieved by incorporating more measurement nodes
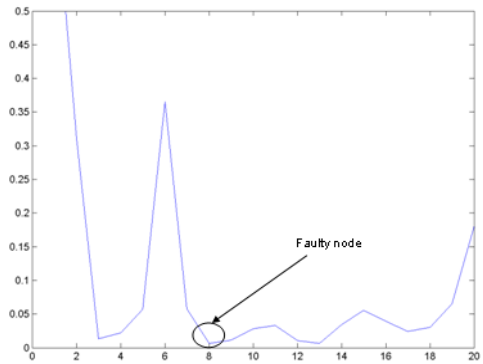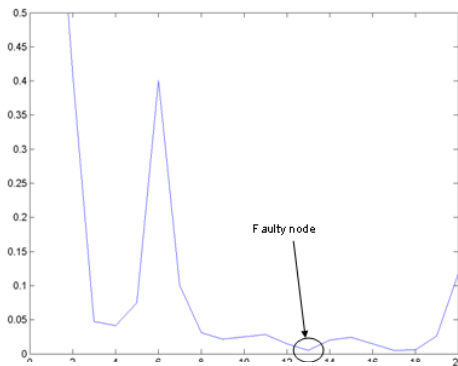
(a)
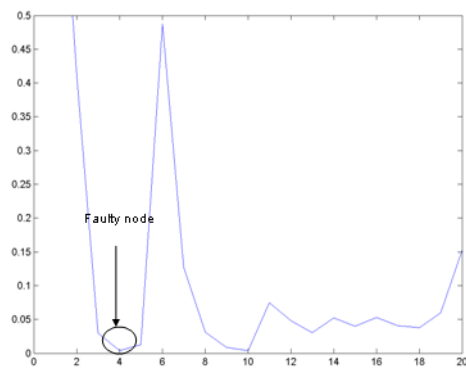
(b)
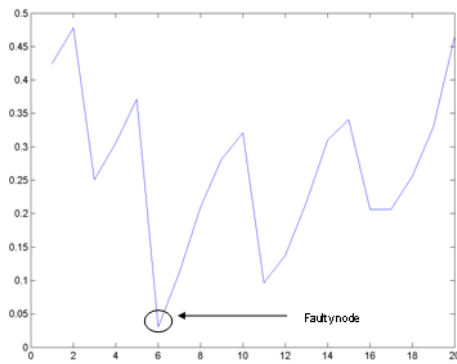
(c)

(d)

(e)

Figure 4.9 Distances between the Measured Pattern (of 4 elements) and the Simulated Patterns in the 20 nodes network(a) Actual short-circuit fault at Node 2 (b) Actual short-circuit fault at Node 4 (c) Actual short-circuit fault at Node 6 (d) Actual short-circuit fault at Node 8 (e) Actual short-circuit fault at Node 13

.

57

4.3.1.2 50 Nodes 5 x10 Network

The equivalent circuit diagram of the mesh network is shown in Figure 4.10. In the hardware testbed, short-circuit fault was created at 20 nodes sequentially. These nodes are marked in red color in the figure. The list of the 20 fault nodes is:

4, 6, 8, 12, 13, 16, 18, 20, 23, 26, 29, 32, 35, 37, 39, 40, 42, 44, 46, 48

For each short-circuit fault, all the node voltages in the testbed were measured. For these 20 "abnormal states", 20 patterns were measured:

$$M_4 \ M_6 \ M_8 \ \dots. \ M_{46} \ M_{48}$$

These 20 patterns share symbol "M" as they were obtained from measurements. Their subscripts denote the actual fault locations.

Signature Pattern Recognition Results By Using a Measured Pattern of 50 elements

Here all the node voltages, that is, voltages at node n1 , n2…n50 are selected to form the "pattern". Hence each measured and simulated pattern is of length 50.

In order to apply the signature pattern recognition algorithm (described in section 4.2.1), a signature dictionary was constructed by simulating the circuit in Figure 4.10with all the 50 possible fault locations. Again, the procedure in section 4.2.1 is followed and the plots of distances between each measured pattern and simulated patterns are shown in Figure 4.11 to Figure 4.14.
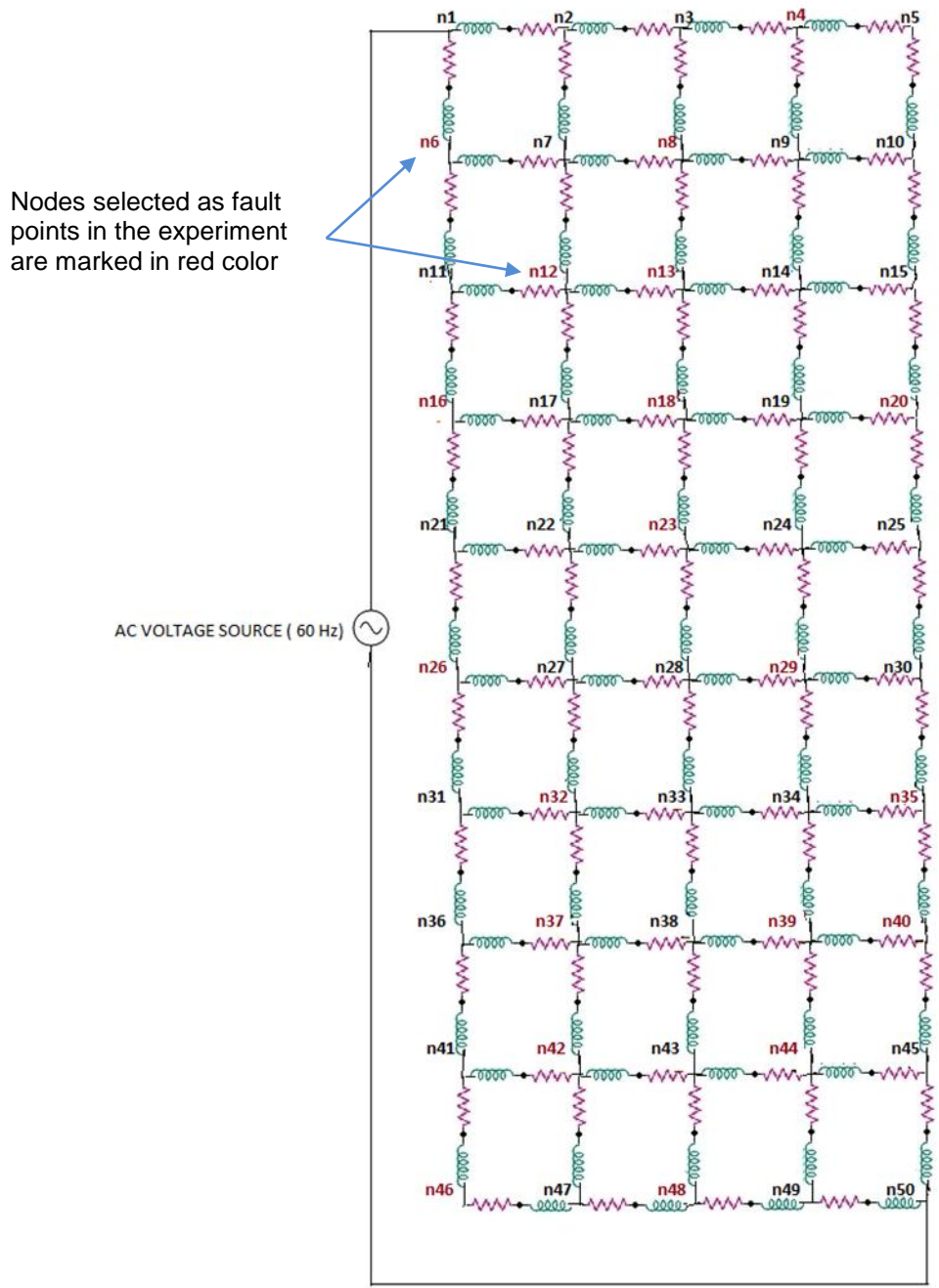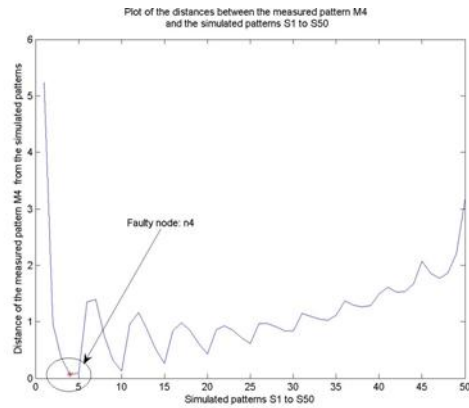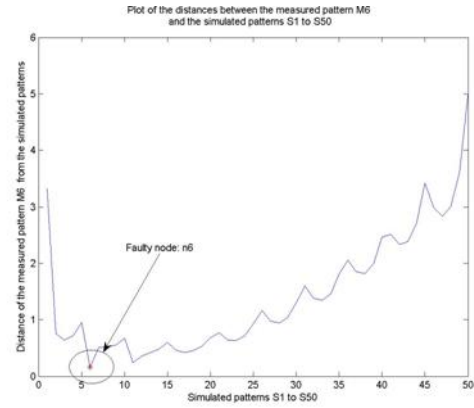
Nodes selected as fault points in the experiment are marked in red color

Figure 4.10 50 node 5x10 network with 20 Short locations

AC VOLTAGE SOURCE (60 Hz)
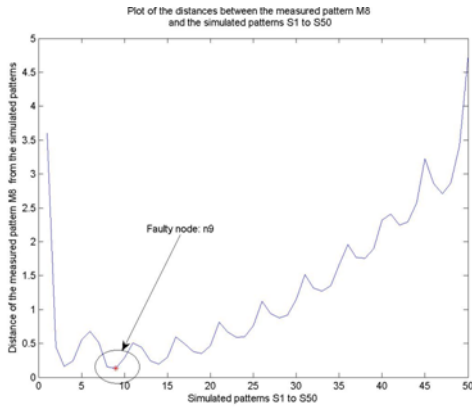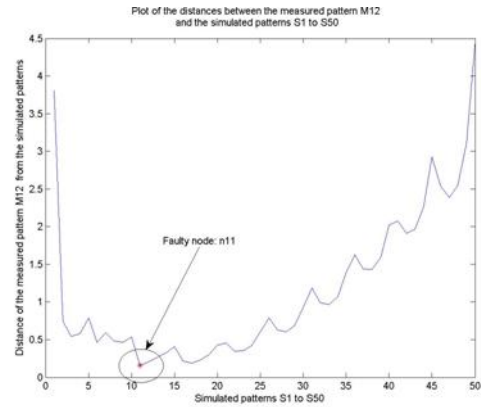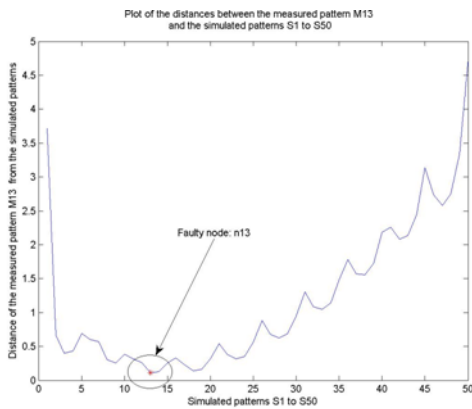
Figure 4.11 Distances between the Measured Pattern (of 50 elements) and the Simulated Patterns in the 50 nodes network (a) Actual short-circuit fault at Node 4 (b) Actual short-circuit fault at Node 6 (c) Actual short-circuit fault at Node 8 (d) Actual short-circuit fault at Node 12 (e) Actual short-circuit fault at Node 13 (f) Actual short-circuit fault at Node 16

Figure 4.12 Distances between the Measured Pattern (of 50 elements) and the Simulated Patterns in the 50 nodes network (a) Actual short-circuit fault at Node 18 (b) Actual short-circuit fault at Node 20 (c) Actual short-circuit fault at Node 23 (d) Actual short-circuit fault at Node 26 (e) Actual short-circuit fault at Node 29 (f) Actual short-circuit fault at Node 32
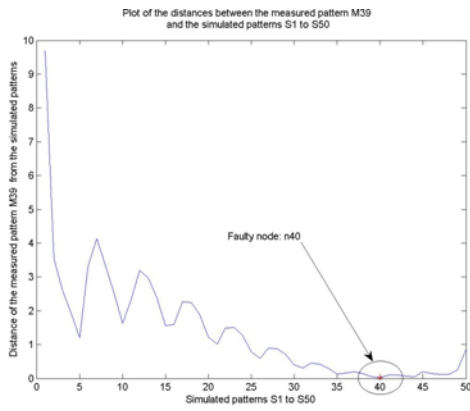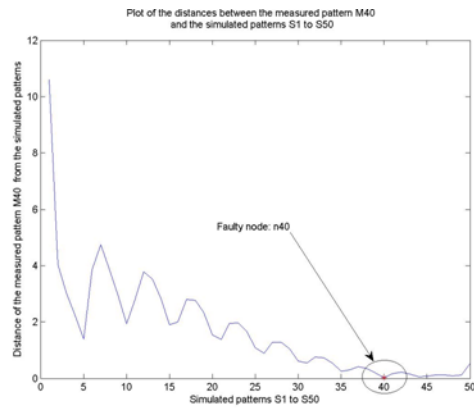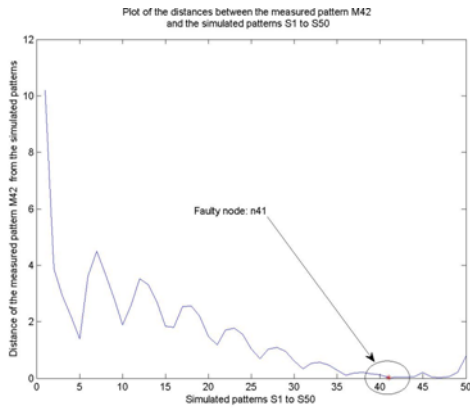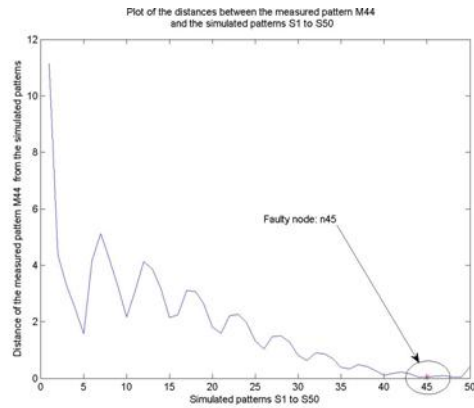
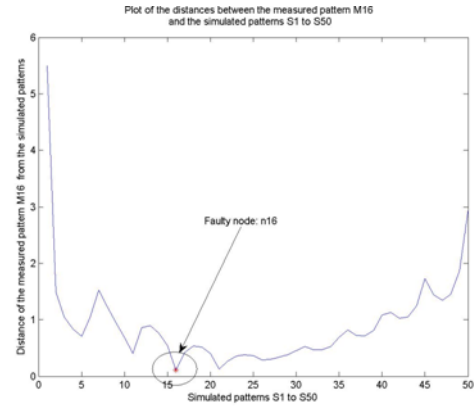Figure 4.13 Distances between the Measured Pattern (of 50 elements) and the Simulated Patterns in the 50 nodes network (a) Actual short-circuit fault at Node 35 (b) Actual short-circuit fault at Node 37 (c) Actual short-circuit fault at Node 39 (d) Actual short-circuit fault at Node 40 (e) Actual short-circuit fault at Node 42 (f) Actual short-circuit fault at Node 45
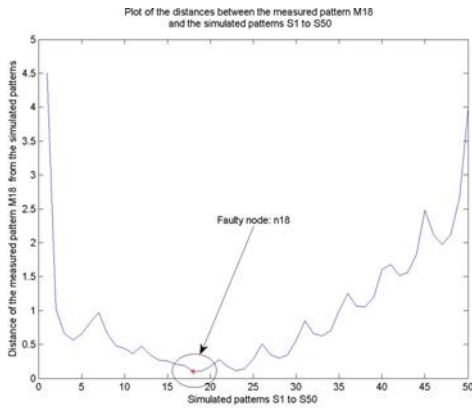
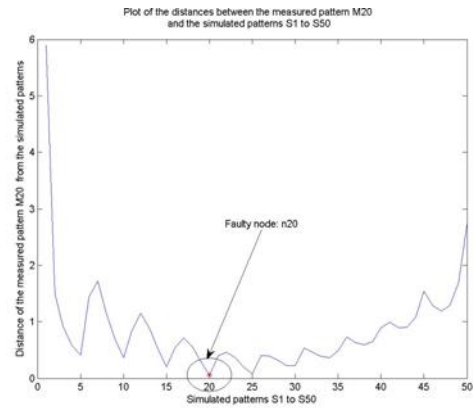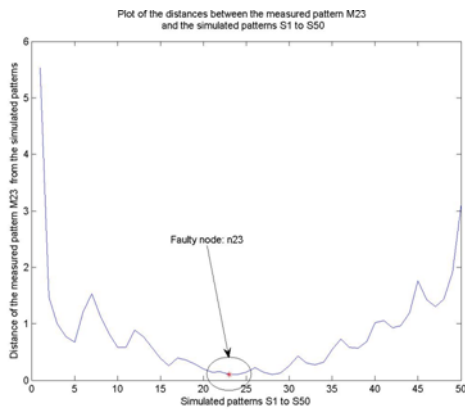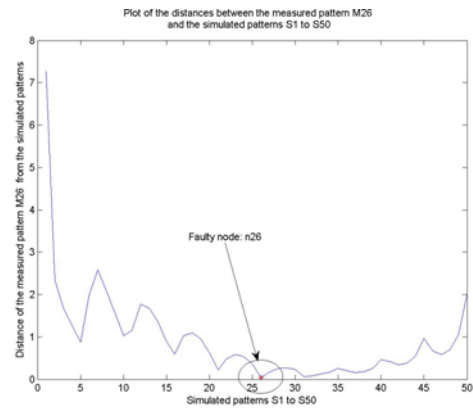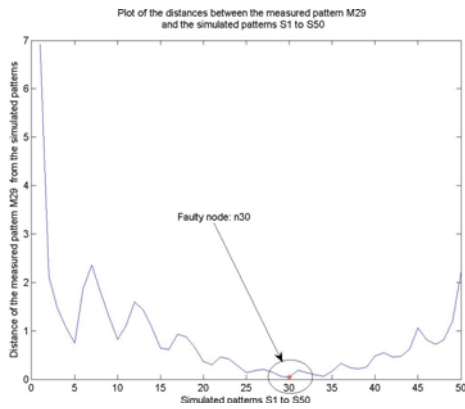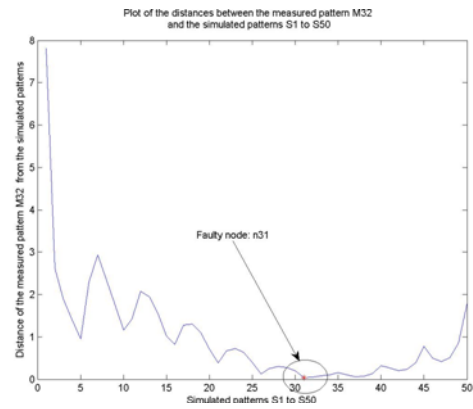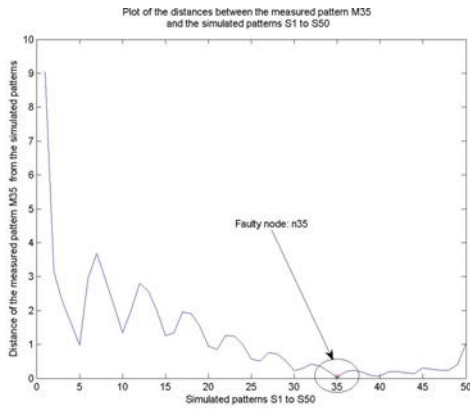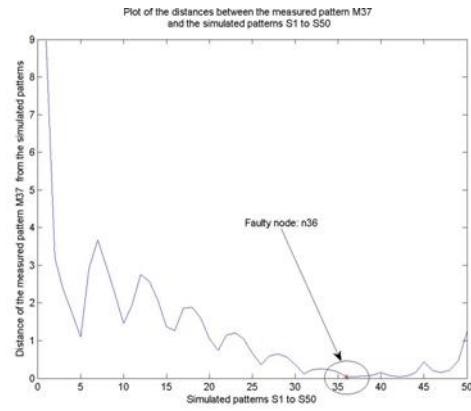(a)   (b)
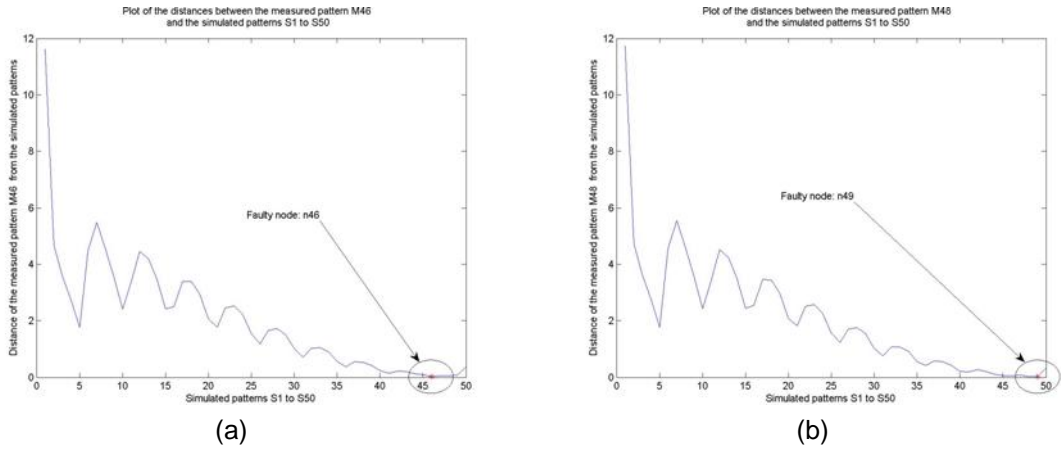
Figure 4.14 Distances between the Measured Pattern (of 50 elements) and the Simulated Patterns in the 50 nodes network (a)Actual short-circuit fault at Node 46 (b) Actual short-circuit fault at Node 48

The localization results in Figure 4.11 to Figure 4.14 are summarized in Table 4.2. Specifically, the fault locations obtained from our pattern recognition algorithm are compared with the actual fault locations. It is observed that, the short circuit faults can be localized with good accuracy. From Table 4.2, the error of our fault localization algorithm is at most one node and hence the fault locations identified by our algorithm are always in the close proximity of the actual fault locations

Table 4.2 Fault localization results using signature pattern recognition algorithm for the 10 x 5 mesh network; GT: Ground truth; ALL: Using measured pattern of 50 elements

GT	4	6	8	12	13	16	18	20	23	26	29	32	35	37	39	40	42	44	46	48
ALL	4	6	**9**	**11**	13	16	18	20	23	26	**30**	**31**	35	**36**	**40**	40	**41**	**45**	46	**49**

Signature Pattern Recognition Results by Using a Measured Pattern of Fewer Elements

As explained in the section 4.2.1.2 , fewer measurement points are chosen to form the "pattern". Two sets of measurement nodes are investigated:

1) Measurement set "S3," in which 16 nodes (about one-third of 50) are selected as the measurement nodes. In this case R = 16 and N =50. Hence the measured and the simulated pattern used for the algorithm are of length 16.

2) Measurement set "M8." This set consists of 8 measurement nodes [6, 5, 25, 27, 41, 49, 35, 38]. In this case R = 8 and N =50. Hence the measured and the simulated pattern used for the algorithm are of length 8

The procedure to calculate the distances between the measured and the simulated patterns is followed. Consider the measured pattern corresponding to actual short-circuit location at Node 23. Specifically, this realistic measured pattern is compared to all the 50 signatures in the dictionary. The comparison results are plotted in Figure 4.15, where the horizontal axis is the index of the 50 signatures and the vertical axis is the distance to the realistic measured pattern. Figure 4.15(a) and Figure 4.15, (b) are obtained with Measurement Set "ALL" and Measurement Set "S3," respectively. Both of them are similar to each other. Both curves show their minimal distances around Node 23, but, quite a few neighbors of Node 23 also exhibit low distances. As a result, it is possible for our pattern recognition algorithm to result in localization inaccuracies in practice.

The above procedure is repeated for all the 20 realistic measurement patterns. The results from our signature pattern recognition algorithm are summarized in Table 4.3

(a)   (b)
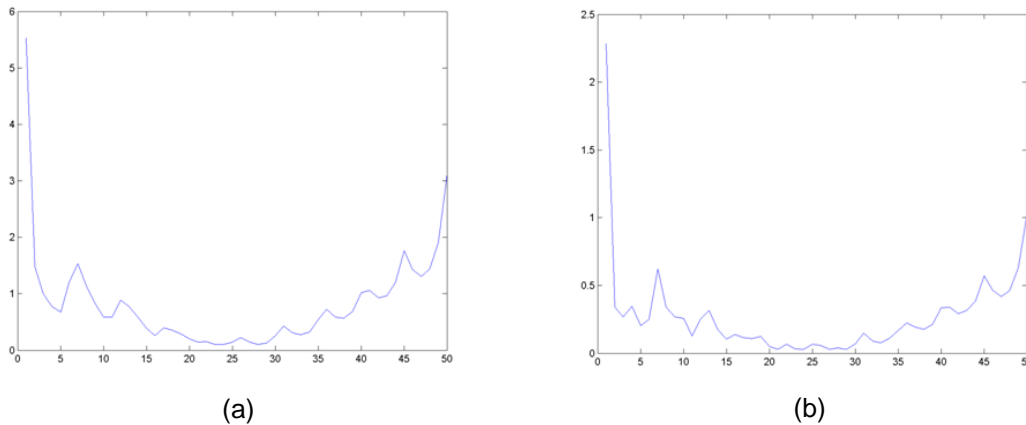
Figure 4.15 The Effect of Reducing the Number of Measurement Points for the Signature Pattern Recognition (a) Using ALL measurements (b) Using measurement set S3

Table 4.3 has four rows. The first row is named "GT": it has the 20 actual (i.e., ground truth) fault locations. The next three rows are localization results obtained from our signature pattern recognition algorithm. These three rows, named "ALL," "S3," and "M8", correspond to Measurement Sets "ALL," "S3," and "M8," respectively. Some localization errors are observed: in Table 4.3 and the errors are marked by bold font. As expected, the fewer the measurement nodes are, the more errors occur. However, it is important to note that, the fault locations identified by our algorithm are always in the close proximity of the actual fault locations, even when errors occur.

Table 4.3 Fault localization results using signature pattern recognition algorithm for the 10 x 5 mesh network.GT: Ground truth; ALL: Using all measurements; S3: Using 1/3 of all measurements; M8: Using 8 measurements

GT	4	6	8	12	13	16	18	20	23	26	29	32	35	37	39	40	42	44	46	48
ALL	4	6	**9**	**11**	13	16	18	20	23	26	**30**	**31**	35	**36**	**40**	40	**41**	**45**	46	**49**
S3	4	6	**3**	**11**	**14**	16	18	20	**21**	26	**30**	32	35	**36**	**44**	40	**41**	**48**	46	48
M8	**10**	6	**3**	**11**	**14**	**21**	**19**	20	**21**	26	**30**	**31**	35	**36**	**40**	40	**47**	**48**	46	**45**

4.3.2 Sparse Sensing

4.3.2.120 Nodes 4 x 5 Network

The Sparse Sensing localization algorithm (described in subsection4.2.2) was applied to Figure 4.7 . In the lab, short circuit was created at 4 points subsequently: Nodes 2, 4, 6, 8, 13.Four nodes (6, 9, 15, and 17) were selected as the measurement nodes. Hence in this case, according to conventions used in section 4.2.2 , m= 20 and c =4. The vector V_0 is of length 4 and the impedance matrix Z_0 is of dimension 4 by 20. Other nodes could be chosen. One practical guideline for node selection is that they should be evenly distributed over the network.

The measured pattern corresponding to actual short-circuit location at Node 13 is processed first. It is assumed that there are two short-circuit faults. Since there are 20 nodes, there exist 20×20 possible "two-fault combinations." The Sparse Sensing algorithm is executed for every of these 20 by 20 combinations.

In Figure 4.16, residue values (defined in Subsection 3.1.3) for all the 20×20 combinations are plotted. In the figure, red color stands for the largest value and blue color stands for the smallest. It is observed from Figure 4.16 that, combination (13, 20) has the smallest residue. Clearly, Node 13 is the actual short-circuit location; whereas Node 20 is the ground and our algorithm identifies Node 20 as a short-circuit as well.
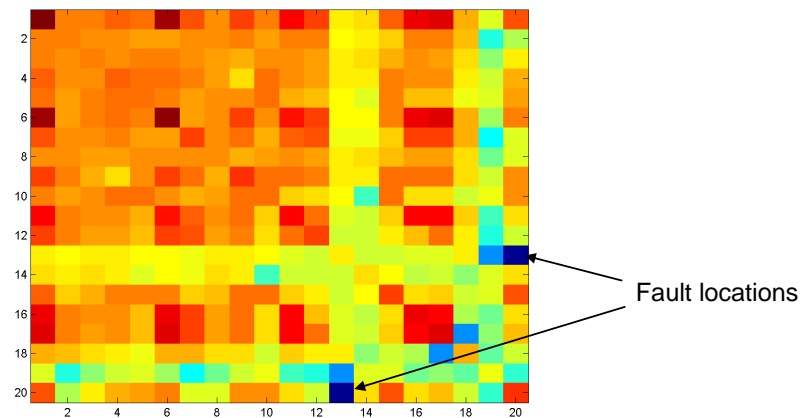

Figure 4.16 Residual Image for Measured Pattern with short-circuit fault at Node 13.

66

The above procedure is repeated for the other four measured patterns (corresponding to actual short-circuit locations at 2, 4, 6, and 8, respectively). Similar residue images are plotted in Figure 4.17. For all of them, our algorithm identifies the fault locations correctly.

(a)   (b)

(c)   (d)
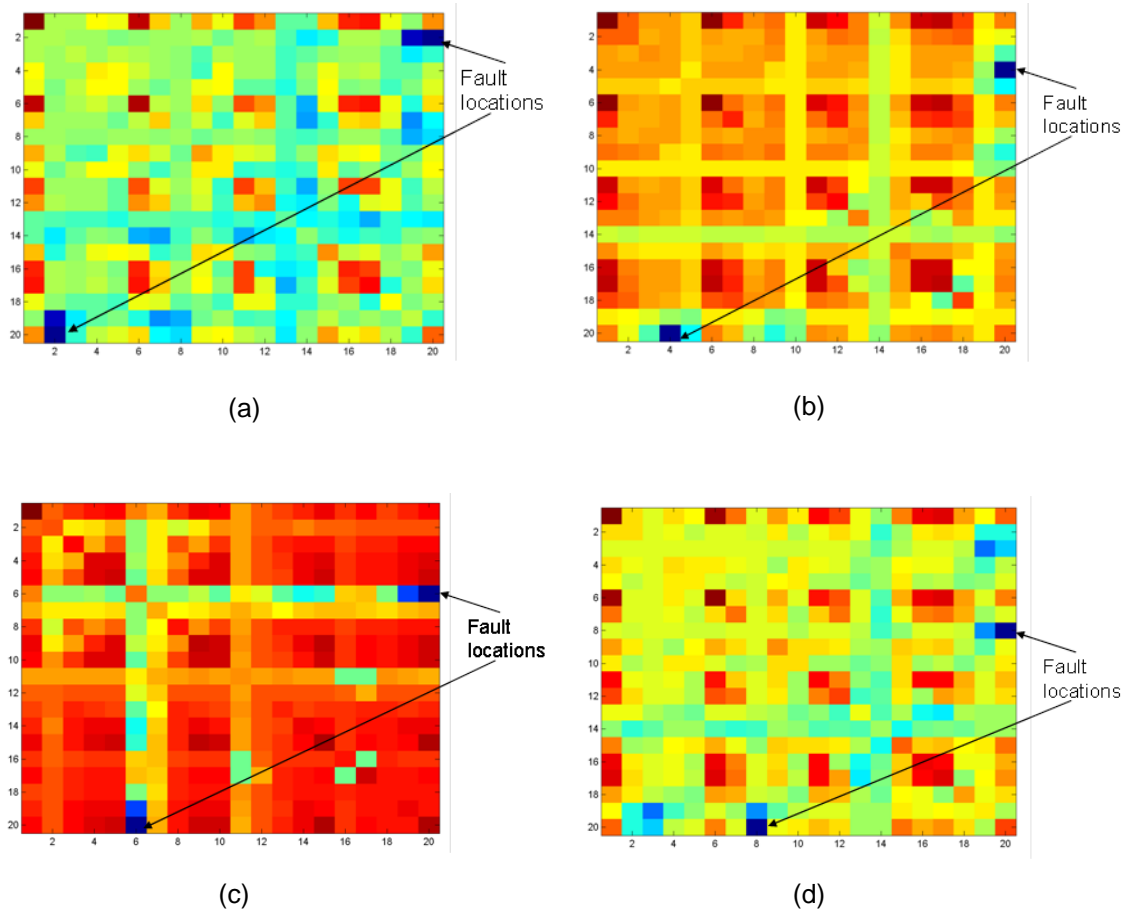
Figure 4.17 Residual images for 4 realistic measured patterns. (a) to (d) correspond to the 4 realistic measured patterns. (a) Actual Short-circuit fault at Node 2 (b) Actual Short-circuit fault at Node 4 (c) Actual Short-circuit fault at Node 6 (d) Actual Short-circuit fault at Node 8

Using the Sparse Sensing algorithm, it has been observed that the localization of short circuit fault can be done with only a small set of measurement points. In the case of Signature Pattern Recognition also, it was found that the fault can be located accurately with 4 measurements in the 20 nodes network. Hence it was important to test the efficiency and

accuracy of this Sparse Sensing algorithm on the bigger 50 nodes network. The next subsection presents the results of the application of Sparse Sensing to detect the fault in the 50 nodes network.

4.3.2.2 50 Nodes 5 x10 Network

The Sparse Sensing localization algorithm (described in subsection 4.2.2) was applied to Figure 4.10. In the lab, a short circuit was created at 20 points on the testbed subsequently. The list of the 20 fault nodes is:

4, 6, 8, 12, 13, 16, 18, 20, 23, 26, 29, 32, 35, 37, 39, 40, 42, 44, 46, 48

Four nodes (6, 5, 41, and 49) were selected as the measurement nodes. Hence in this case, according to conventions used in section 4.2.2 , m = 50 and c = 4. The vector V_0 is of length 4 and the impedance matrix Z_0 is of dimension 4 by 50. The realistic measured pattern corresponding to actual short-circuit location at Node 23 is analyzed first. It is assumed that there is only one fault in the network. In Figure 4.18, the residue values (defined in Subsection 4.2.2) with respect to all the 50 nodes in the network are plotted. The residue at Node 23 is substantially smaller than all the others and hence it is chosen as the fault node.
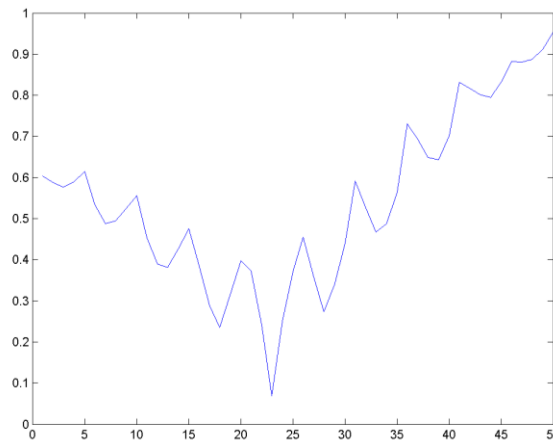

Figure 4.18 Residual plot for realistic measured pattern with short-circuit fault at Node 23 using sparse sensing algorithm. Horizontal axis stands for the 50 nodes in the network; the vertical axis stands for the residue value

Comparison between Figure 4.18 and Figure 4.15 indicates that the sparse sensing algorithm is superior to the pattern recognition algorithm, especially after considering the fact that only 4 measurement nodes are employed in the sparse sensing algorithm. This conclusion is further supported by results from other realistic measured data. Figure 4.19 to Figure 4.22 show residual plots similar to that in Figure 4.18. These plots correspond to realistic measured patterns with fault located at the rest of the nodes apart from node 23. Again, only 4 measurement nodes (Nodes 6, 5, 41, and 49) are used in the sparse sensing algorithm. In all the four plots, the actual fault locations are exactly identified without any ambiguities.

(a)

(b)

(c)

(d)

Figure 4.19 Residual plot for realistic measured pattern using Sparse Sensing algorithm (a) Actual Short-circuit fault at Node 4 (b) Actual Short-circuit fault at Node 6 (c) Actual Short-circuit fault at Node 8 (d) Actual Short-circuit fault at Node 12
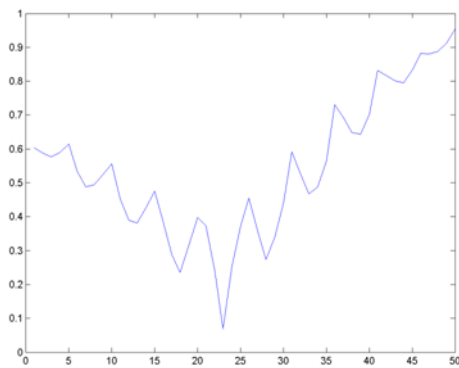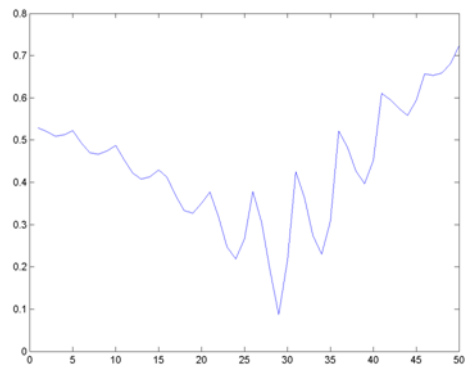
Figure 4.20 Residual plot for realistic measured pattern using Sparse Sensing algorithm (a) Actual Short-circuit fault at Node 13 (b) Actual Short-circuit fault at Node 16 (c) Actual Short-circuit fault at Node 18 (d) Actual Short-circuit fault at Node 20 (e) Actual Short-circuit fault at Node 26 (f) Actual Short-circuit fault at Node 29
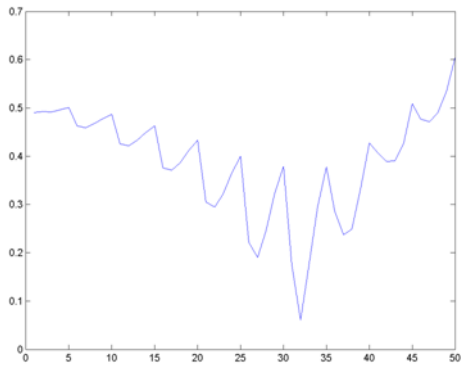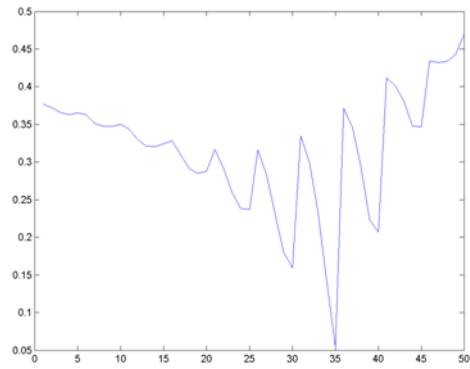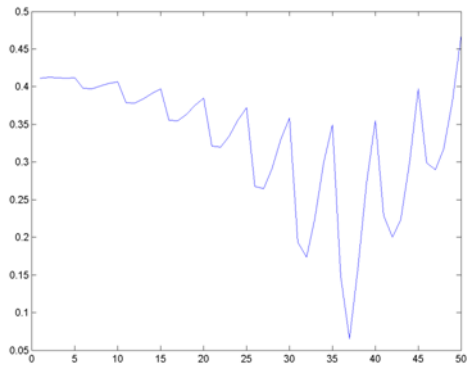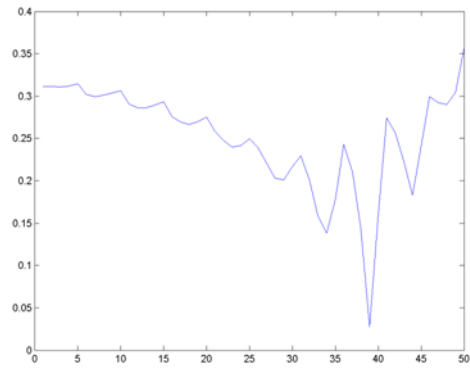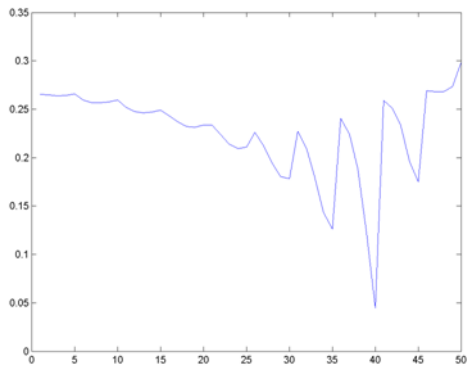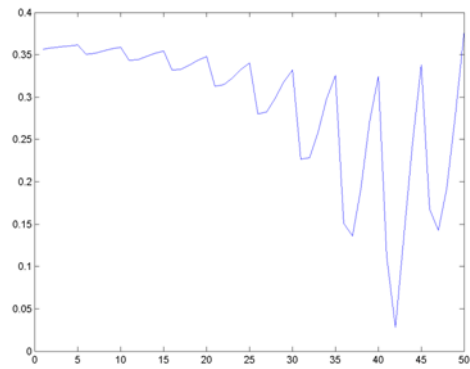
Figure 4.21 Residual plot for realistic measured pattern Sparse Sensing algorithm(a) Actual Short-circuit fault at Node 32 (b) Actual Short-circuit fault at Node 35 (c) Actual Short-circuit fault at Node 37 (d) Actual Short-circuit fault at Node 39 (e) Actual Short-circuit fault at Node 40 (f) Actual Short-circuit fault at Node 42
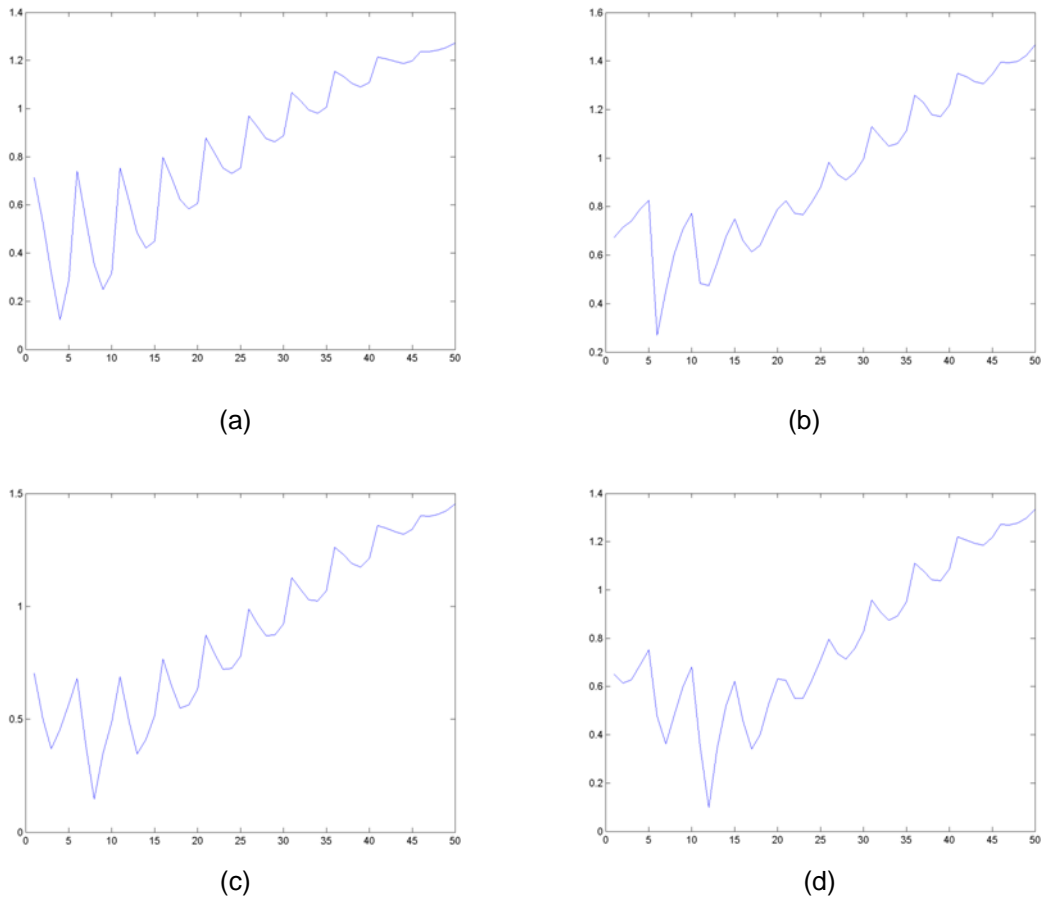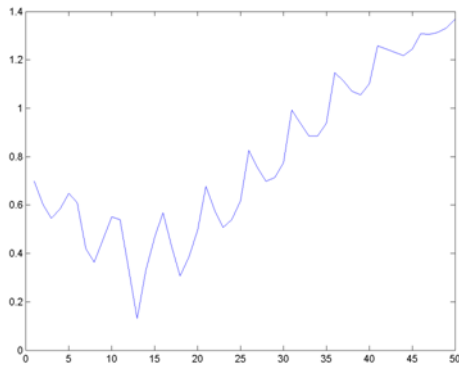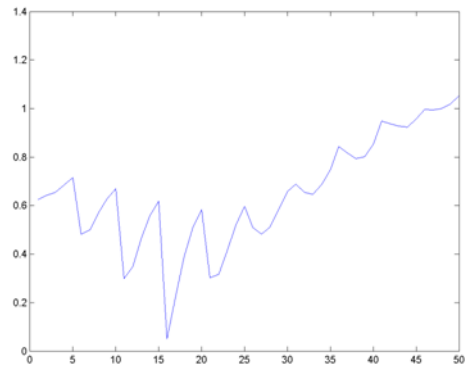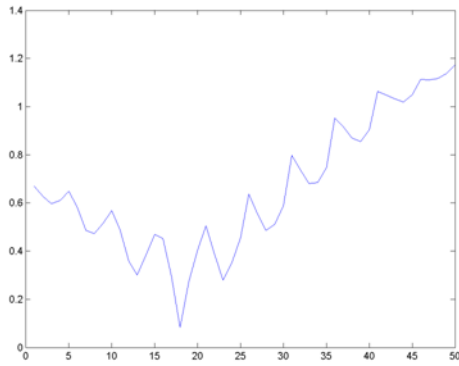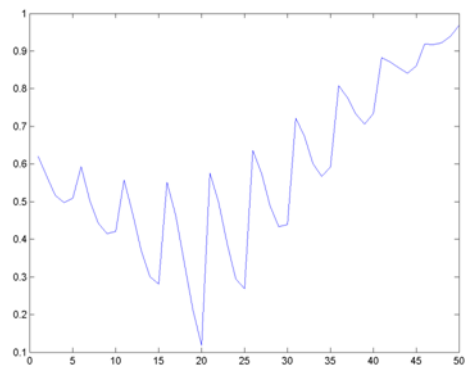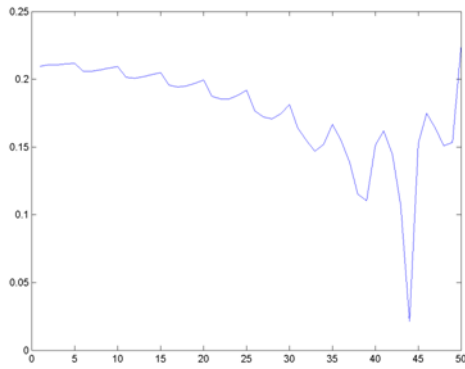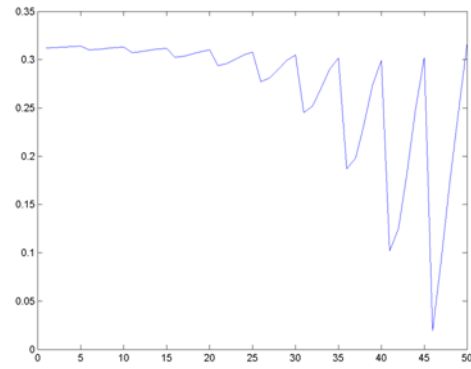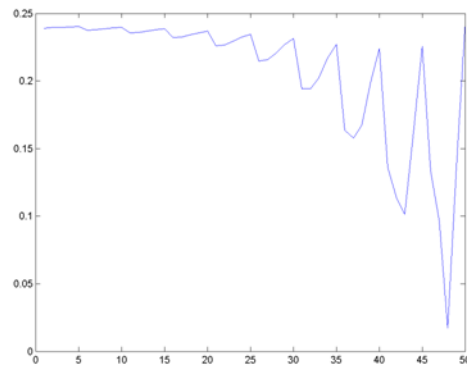
Figure 4.22 Residual plot for realistic measured pattern using Sparse Sensing algorithm(a) Actual Short-circuit fault at Node 44 (b) Actual Short-circuit fault at Node 46 (c) Actual Short-circuit fault at Node 48

After the sparse sensing algorithm is applied to all the 20 realistic measured patterns, its fault localization results are summarized in Table 4.4. It has two rows. The first row is named "GT": it has the 20 actual (i.e. ground truth) fault locations. The second row contains localization results obtained from our sparse sensing algorithm. The second row is named "S4" because only four measurement nodes (6, 5, 41, and 49) are employed.

Table 4.4 Fault localization results using sparse sensing algorithm for the 10 x 5 mesh network.GT: Ground truth; S4: From sparse sensing algorithm using 4 measurement nodes

GT	4	6	8	12	13	16	18	20	23	26	29	32	35	37	39	40	42	44	46	48
S4	4	6	8	12	13	16	18	20	23	26	29	32	35	37	39	40	42	44	46	48

The results of short circuit fault at Nodes 8, 12, 39, and 44 using the Signature Pattern Recognition appear prone to errors in Table 4.3. However, as it can be seen from the above results that the faults at nodes 8, 12, 39, and 44 are accurately determined by Sparse Sensing method. The comparison between Table 4.3 and Table 4.4 confirms that the sparse sensing algorithm is more robust than the Pattern Recognition algorithm.

According to the numerical and experimental studies, the Sparse Sensing algorithm exhibits excellent performance when the number of fault nodes is small. When there are one or two faults, faults can be precisely localized within 50 ms (corresponding to 3 cycles at 60 Hz). However, if there exist a large number of fault nodes (which is not very common in realistic power distribution networks), exhaustive search becomes inefficient.

Multiple Fault Localization in the 50 nodes 10 x 5 mesh network

The Sparse Sensing algorithm can also be used to detect multiple faults in the network. This property of the algorithm was tested by creating two fault points in the 50 node network. The first node and the last node were connected to generator and ground respectively. There were two fault nodes: node 12 and node 38. The measurements of 16 nodes, i.e. 2, 5, 8, 11,, 48 were used. Hence in this case m=50 and c =16. The procedure in section 4.2.2 is followed and Figure 4.23 shows the sparse sensing results, assuming the last node is a ground node, not a faulty node. From the figure, we can see the sparse sensing method correctly identifies two fault locations: 12 and 38.
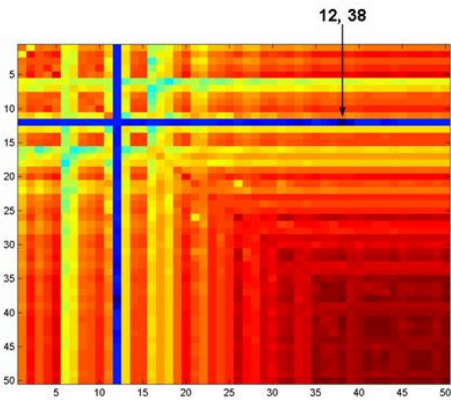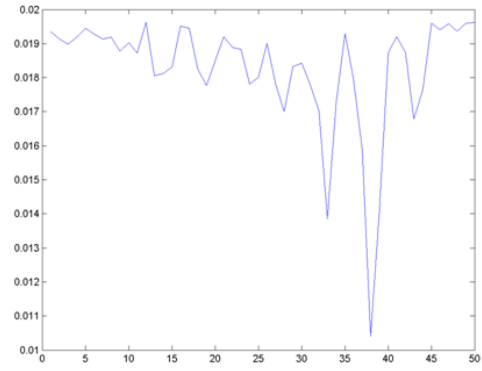
Figure 4.23 Localization of Multiple Faults in the 50 node network using Sparse Sensing (a) Two faults residual image (b) The residual plots of 12-th row of (a)

CHAPTER 5

SUMMARY AND SCOPE FOR FUTURE DEVELOPMENT

5.1 Summery

This thesis summarizes the research efforts on localizing short-circuit faults in power distribution networks. Specifically, an experimental testbed is constructed to emulate realistic power distribution networks; various short-circuit faults are artificially created in the testbed; voltages/currents are measured over the testbed; and finally, fault localization is achieved by analyzing the measurement data. Two types of power distribution networks are analyzed: serial/radial and grid/mesh networks.

For the radial/serial network, both zero impedance and impedance faults are studied. The scheme for zero impedance faults make use of measurements at only one terminal. The scheme proposed for non-zero impedance fault involves measurements at two terminals; and, fault location is estimated from the intersection of forward voltage profile and backward voltage profile. The localization results from our experimental data are accurate with errors of at most three nodes.

In the case of mesh/grid network, two novel algorithms have been developed: signature pattern recognition and sparse sensing. The signature pattern recognition algorithm employs "signatures" composed of voltage magnitudes over the network, whereas the sparse sensing algorithm takes advantage of the fact that the current vector derived from the Kirchhoff's equations must be a sparse vector. Both algorithms have shown excellent results to localize short faults in a mesh network. According to extensive experiments, the localization accuracy based on signature pattern recognition is greatly affected by the number of measurement points. Whereas, the sparsity sensing algorithm demonstrates nice performance consistently

even with a small amount of measurement points. Typically for the same network configuration, the sparsity sensing algorithm is capable of localizing the faults with fewer measurements than the signature pattern recognition algorithm. As a conclusion, the sparsity sensing algorithm is more robust.

5.2 Scope for future development

This research can serve as the groundwork for further efforts towards precise and efficient schemes for fault localization in power system. In the future, techniques will be sought for fault localization in noisy environments. The criteria to determine the optimal measurement nodes in practical noisy environments are the major research task. In the signature pattern recognition algorithm, methods other than least-square could be tested to find the closest match between the measured and simulated pattern. As for the sparse sensing algorithm, the sparsity-based L1 solvers, such as the one in [28], could be incorporated into the algorithm to further enhance its accuracy and efficiency. Also, 3-phase testbed could be built in the lab and the algorithms could be implemented in real-time by using a data acquisition system with voltage sensors, signal conditioning circuit, and microcontrollers for data processing.

APPENDIX A

MEASUREMENT DATA FOR THE LOCALIZATION OF IMPEDANCE FAULTS IN THE SERIAL
DISTRIBUTION NETWORK

Measurement data for Figures 4 to 6 are listed in the following table. In the table, "V_{supply}" is the voltage to the left of R_0, "V_{in}" is the voltage to the right of R_0 and "V_L" is the voltage at the load or the end point voltage. Phase difference between V_{supply} and V_{in} are given in the 5th column and 6th column. The 5th column records which voltage's phase leads and the 6th column is the time delay between V_{supply} and V_{in}. The difference between V_{supply} and V_{in} is the voltage drop across R_0, based on which the current over R_0, is calculated in our post-processing.

Measurement number	R_{fault} in ohms	$|V_{supply}|$ in volts	$|V_{in}|$ in volts	Which leads (V_{supply} or V_{in})	Time in ms	$|V_L|$ in volts	Actual fault location (in terms of number of cells from supply side)
1		1.082	0.594	V_{supply}	0.943	0.1751	5
2		1.675	1.265	V_{supply}	0.68	0.152	12
3	0.51	1.91	1.52	V_{supply}	0.58	0.15	15
4		2.18	1.78	V_{supply}	0.517	0.148	18
5		2.5	2.145	V_{supply}	0.445	0.14	22
6		3.145	2.805	V_{supply}	0.348	0.142	30
7		1.426	0.922	V_{supply}	0.432	0.556	5
8		1.965	1.49	V_{supply}	0.456	0.54	12
9	1.59	2.21	1.775	V_{supply}	0.417	0.53	15
10		2.44	2.03	V_{supply}	0.39	0.54	18
11		2.735	2.36	V_{supply}	0.358	0.52	22
12		3.35	2.99	V_{supply}	0.305	0.524	30
13		1.937	1.387	V_{supply}	0.201	1.07	5
14		2.395	1.925	V_{supply}	0.272	1.056	12
15	3.08	2.6	2.17	V_{supply}	0.274	1.044	15
16		2.815	2.385	V_{supply}	0.276	1.038	18
17		3.09	2.68	V_{supply}	0.265	1.03	22
18		3.655	3.29	V_{supply}	0.234	0.99	30

.

REFERENCES

[1]   T. A. Short, "Electric Power Distribution Handbook" , CRC Press 2003
[2]   C37.100-1992 IEEE Standard Definitions for Power Switchgear 1992
[3]   W. Lee, "Arcing Fault Detection and Location in Secondary Distribution Networks by On-Line RMS Processing," Final Report to Con Edison, December 1998.
[4]   Rodrigo Hartstein Salim, "Extended Fault-Location Formulation for Power Distribution Systems", IEEE Transactions On Power Delivery, Vol. 24, No. 2, April 2009
[5]   Arturo Suman Bretas, "Fault Location in Unbalanced DG Systems using the Positive Sequence Apparent Impedance"
[6]   K.Ferreira, "Fault Location for Power Transmission Systems Using Magnetic Field Sensing Coils," Master Thesis, April 2007.
[7]   H . Lee Willis, " Power Distribution Planning Reference Book, Second Edition", CRC Press 2004
[8]   William H. Kersting, Distribution System Modeling and Analysis, 2nd Edition, CRC Press, 2006, PP. 1-5, 79, 88, 95, 407-408.
[9]   Madhab Paudel, "Development of a Fault Location Algorithm Based on Distributed Neutral-to-Ground Current Sensor Measurements", Master's Thesis, 2009, South Dakota State University.
[10]   Burke, J. J. and Lawrence, D. J., "Characteristics of Fault Currents on Distribution Systems," IEEE Transactions on Power Apparatus and Systems, vol. PAS-103, no. 1, pp. 1–6, January 1984. EPRI 1209-1 (1983).
[11]   IEEE Guide for the Application of Faulted Circuit Indicators for 200 A, Single-Phase Underground Residential Distribution (URD)
[12]   F. Han, X. Yu, M. Al-Dabbaghl, Y. Wang, "Fault location in power distribution networks using sinusoidal steady state analysis," Proceedings of the 7th Asia Pacific Complex Systems Conference, 2004
[13]   Qais Hashim Alsafasfeh, "Pattern Recognition for Fault Detection, Classification and Localization in Electrical Power Systems" , PhD dissertation, 2010, Western Michigan University.
[14]   M.-S. Choi, S.-J. Lee, D.-S. Lee, and B.-G. Jin, "A new fault location algorithm using direct circuit analysis for distribution systems," IEEE Trans. Power Del., vol. 19, no. 1, pp. 35–41, Jan. 2004.
[15]   IEEE Guide for Determining Fault Location on AC Transmission and Distribution Lines, IEEE Std. C37.114-2004,.
[16]   J. Zhu, D. L. Lubkeman, and A. A. Girgis, "Automated fault location and diagnosis on electric power distribution feeders," IEEE Trans. Power Del., vol. 12, no. 2, pp. 801–809, Apr. 1997

[17]   Rodrigo Hartstein Salim, "Extended Fault-Location Formulation for Power Distribution Systems", IEEE Transactions on Power Delivery, Vol. 24, No. 2, Apr 2009

[18]   H. Mokhlis, "Locating Fault Using Voltage Sags Profile for Underground Distribution System", 2010 International Conference on Power System

[19]   "Smart grid sag and temperature monitor for overhead power lines," DOE Phase I Abstract in DOE SBIR Website, 2010.

[20]   A. Livshitz, B. H. Chudnovsky, B. Bukengolts, and B. A.Chudnovsky, "On-line temperature monitoring of power distribution equipment," presented at IEEE Industry Applications Society 52nd Annual Petroleum and Chemical Industry Conference, Denver, CO, September 2005.

[21]   Samson,   Fast   response   temperature   sensor, http://www.samson.de/pdf_en/t52040en.pdf

[22]   W. Charytoniuk, Wei-Jen Lee, M. S. Chen, J. Cultrera, T. Maffetone, "Arcing Fault Detection in underground Distribution Networks -Feasibility Study", IEEE-IAS, I&CPS Annual Conference. Clearwater Beach, FL. May 2000, pp15-20

[23]   Highly multiplexed, low cost fiber-optic sensor array for underground cables condition monitoring," DOE Phase I DOE Phase I Abstract in DOE SBIR Website, Intelligent Fiber Optic Systems Corporation, 2010.

[24]   T. H. Chen, M. S. Chen, Wei-Jen Lee, Paul Kotas, Pete Van Olinda, "Distribution System Short Circuit Analysis - A Rigid Approach," Power Industry Computer Applications Conference, Baltimore, IEEE Transactions on Power Systems. Feb. 1992, pp444 - 450.

[25]   H. Saada, Power System Analysis, McGraw Hill, 1999.

[26]   J. J. Grainger and W. D. Stevenson, Power System Analysis, McGraw Hill, 2004M. Elad, *Sparse and Redundant Representations*, Springer, 2010.

[27]   J. D. Glover, M.S. Sarma, and T. J. Overbye, Power System Analysis and Design, Thompson, 2008..

[28]   Qiaohui Hu, "Distribution Network Contingency Analysis and Contingency Detection with the consideration of Load Models", PhD dissertation, August 2010, The University of Texas at Arlington

[29]   M. Elad, Sparse and Redundant Representations, Springer, 2010.

BIOGRAPHICAL INFORMATION

Omkar Limaye was born in Thane city in Maharashtra, India in 1987. He received his B.Tech. Degree in Electrical Engineering from Veermata Jijabai Technological Institute (VJTI), Mumbai in July 2009. He is currently pursuing a Master of Science degree in Electrical Engineering at The University of Texas at Arlington. His research interests include Power System Protection and Relaying, Embedded Microcontrollers and Control Systems.

Mr. Limaye is a member of IEEE ETA KAPPA NU (HKN) Honor Society. He was the recipient of the second prize in the graduate student poster contest held at IEEE PSCE 2011 held in Arizona, US.